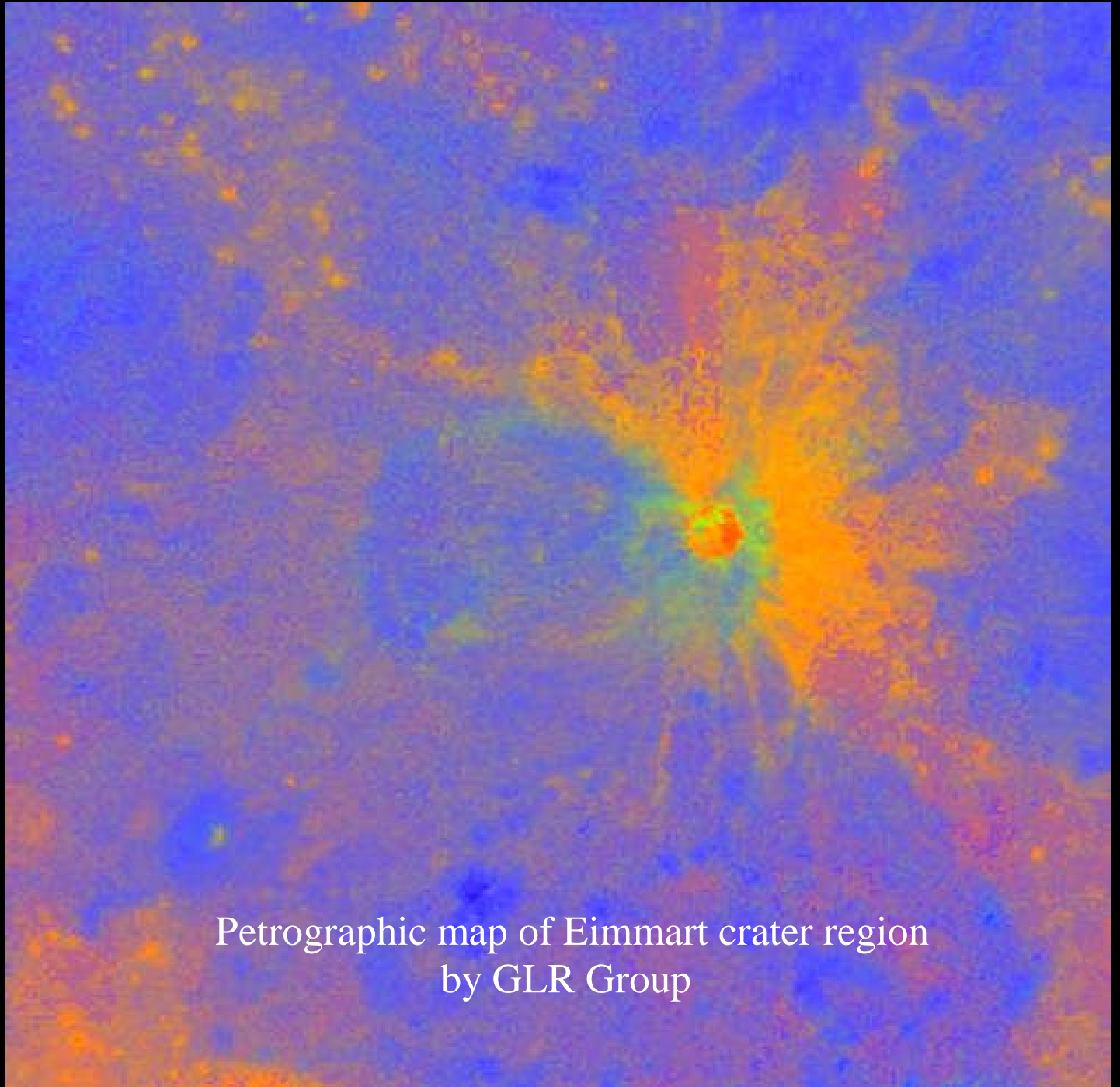


Selenology Today 19



Manual for Lunar Spectral Work



Selenology Today is devoted to the publication of contributions in the field of lunar studies.

Manuscripts reporting the results of new research concerning the astronomy, geology, physics, chemistry and other scientific aspects of Earth's Moon are welcome.

Selenology Today publishes papers devoted exclusively to the Moon.

Editor-in-Chief:

R. Lena

Reviews, historical papers and manuscripts describing observing or spacecraft instrumentation are considered.

Editors:

M.T. Bregante

The Selenology Today

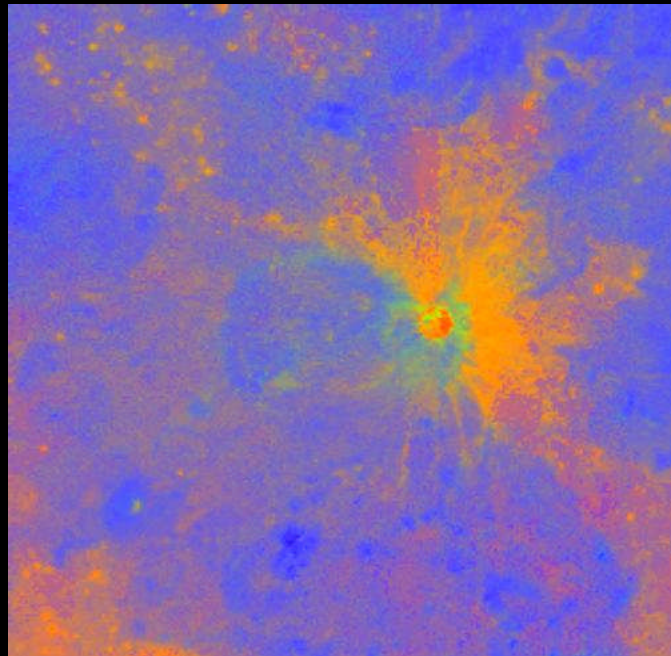
Editorial Office

J. Phillips

selenology_today@christian-woehler.de

C. Wöhler

C. Wood



**Manual for Lunar
Spectral Work
Selenology Today 19**

Geological Lunar Research Group (GLR)

Manual for Lunar Spectral Work

Richard Evans

Raffaello Lena

Christian Wöhler

The instructions and programming code and any other materials present in this paper or provided by Selenology Today are for use solely at the users risk and come with no guarantee that they will work on your system. The risk of using this material lies entirely with the user. The material has so far been tested only on a Windows XP operating system and possible problems or adverse effects on other systems have not been evaluated.

Preface

GLR is an organization dedicated to lunar scientific studies of all types but particularly to studies of lunar domes and lunar geology. Most GLR members are amateur astronomers or amateur geologists and many have a background in science, mathematics and/or computer studies.

During the past several years, a spectral working group within GLR has become increasingly interested in lunar geologic studies using remote sensing (<http://rst.gsfc.nasa.gov/>). Remote sensing of the moon involves acquiring spectra of the lunar surface using a variety of instruments. As experience with spectra was gained by the group, a number of articles dealing with lunar spectra have been published in Selenology Today and other journals. Experience was gained in both Earth based remote sensing using spectrographs or band interference filters at the telescope and in interpretation of spectral band images taken by the lunar probes. In particular the group has worked with data acquired by Clementine and Lunar Prospector (<http://www.mapaplanet.org/explorer/moon.html>), and most recently by Selene (<https://www.soac.selene.isas.jaxa.jp/archive/>).

Remote lunar sensing typically involves acquisition of lunar spectra at UV-VIS-NIR wavelengths (Clementine and Selene) or using a gamma ray spectrometer (Lunar Prospector) although many other wavelengths and techniques can be used. GLR has become interested in a wide variety of spectral issues ranging from their acquisition and calibration to their application in understanding the rock and mineral composition of the lunar surface. A great deal of experience has been gained by GLR in these areas over the years. Because of the perceived complexity of lunar spectral studies and the lack of availability of good reference material written at a basic level, this exciting field remains “terra incognita” to most amateur astronomers.

This Spectral Manual was written in an attempt to educate amateur astronomers in lunar spectral studies and lunar geology and to make this field more accessible to them. The emphasis is on the determination of the rock and mineral composition of the lunar surface using spectral studies. This initial edition of the manual assumes that the reader has at least a rather basic knowledge of mathematics, limited computer skills, and at least some very basic familiarity with the moon and with current thinking about its composition. Hopefully future editions will evolve which will make the manual even more readable by those with little or no grounding in science or mathematics.

The Spectral Manual discusses the acquisition and calibration of spectral images, generation and interpretation of pixel block spectra from spectral images, identification and mapping of spectral parameters, enhancing the resolution of lunar prospector elemental abundance data, and the creation of lunar petrographic maps. Hopefully this will provide a lot of new information to amateur lunar enthusiasts having an interest in lunar geology, and will make it possible for them to explore this exciting field.

Finally, I would like to thank Raffaello Lena (the founder of GLR) for his continued efforts to make spectral studies an important component of the ongoing research activity of GLR. This manual would not have been possible without his hard work, leadership and dedication to the amateur astronomy community. Anyone who finds this manual useful and discovers that suddenly new horizons in lunar research (previously lying only in shadow) have become accessible... owes Raf a debt of gratitude.

Rick Evans, GLR member

Contents

>1. History of Lunar Spectral Work

>2. Mineralogical properties and spectral data

>2.1 Primer on Lunar Geology

>3. Preparation and Significance of Ratio Images

>4. Introduction to Lunar Spectra

>5. Working with Spectra

>6. Clementine Five Band UVVIS Spectra

>7. Alternate Calibrations of Clementine UVVIS+NIR Imagery

>8. FeO and TiO₂ Estimation Using Clementine Band Images

>9. Spectral Parameter Mapping in Octave

>10. Production of Elemental Abundance Maps in Octave

>11. Working with Selene Imagery

>12. Conclusion

> Appendix 1

>1. History of Lunar Spectral Work

Although the existence of the lunar regolith was predicted by infrared studies of the Moon in 1948, technological advancements produced little progress in the interpretation of lunar spectra prior to the 1960s. Lunar spectra were simply viewed as reflected solar spectra since no differences in the number or wavelength of Fraunhofer absorption bands was present. In 1968, John B. Adams wrote a landmark paper in *Science* in which he described the spectral identification of various lunar minerals containing iron by the presence of an absorption trough near 1000 nm. This method, capable of identifying various lunar pyroxenes and olivine, has been used successfully for many years.

The return of Apollo lunar samples in 1969 enabled laboratory analysis of lunar minerals and provided a basis for better calibration of telescope based spectroscopy. Technological advances in spectroscopy design, filter construction and the advent of CCD imaging have enabled a rapid advance in lunar geologic studies. In particular, remote sensing using individual interference filters or tunable filters has facilitated imaging at discrete wavelengths of light and has greatly increased spatial resolution in spectral studies of the lunar surface. Since the 1990s a number of sophisticated lunar probes such as Clementine, Lunar Prospector, Galileo, Selene, Chandrayaan, and others have added substantially to our understanding of lunar composition. Such probes eliminate the problem of spectral absorption caused by the Earth's atmosphere which can make terrestrial telescopic imaging at ultraviolet and infrared wavelengths difficult.

Today, amateur astronomers having a modest background in mathematics and the physical sciences and equipment amounting to little more than a computer and internet connection can make useful contributions to our understanding of lunar geology using readily

available spectral data and public domain software.

>2. Mineralogical properties and spectral data

The spectra presented in this section are available on the World Wide Web site: <http://speclab.cr.usgs.gov>

Other spectral libraries include the mid-infrared work of Salisbury et al., (1991). A recently available spectral library web site is the NASA ASTER site (<http://asterweb.jpl.nasa.gov>), managed by Simon Hook, Jet propulsion Laboratory.

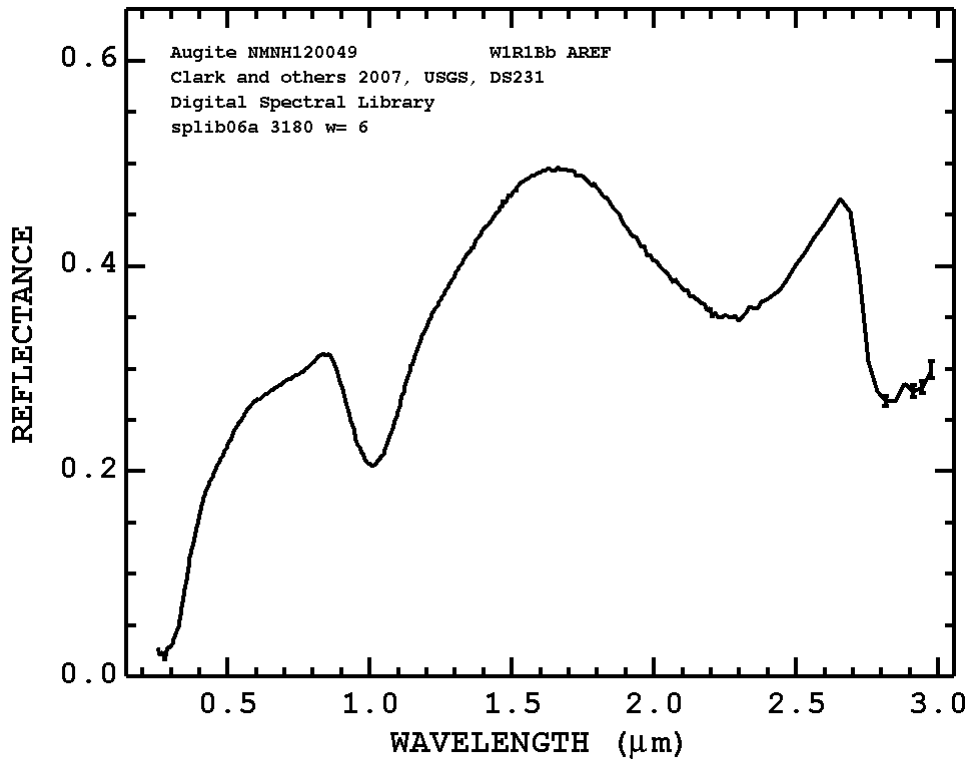
Pyroxenes

Pyroxenes are the most abundant ferromagnesian silicate minerals on the Earth and the Moon. Pyroxene compositions fall largely into the subset of the ternary system MgSiO_3 - CaSiO_3 - FeSiO_3 below 50 mole% CaSiO_3 .

This ternary field is bounded by the compositions :

$\text{CaMgSi}_2\text{O}_6$ (diopside)- $\text{CaFeSi}_2\text{O}_6$ (hedenbergite)- MgSi_2O_6 (enstatite)- FeSi_2O_6 (ferrosilite).

Clinopyroxenes have general formula $(\text{Ca,Mg,Fe})_2\text{Si}_2\text{O}_6$, with small amounts of Al, Mn and Na substituting for other elements. The most significant clinopyroxene endmember is diopside, $\text{CaMgSi}_2\text{O}_6$. Augite is the intermediate member of the series. However, augite is not just an intermediate, but is unique in that it contains percentages of sodium and aluminum that are mostly lacking in diopside and hedenbergite.

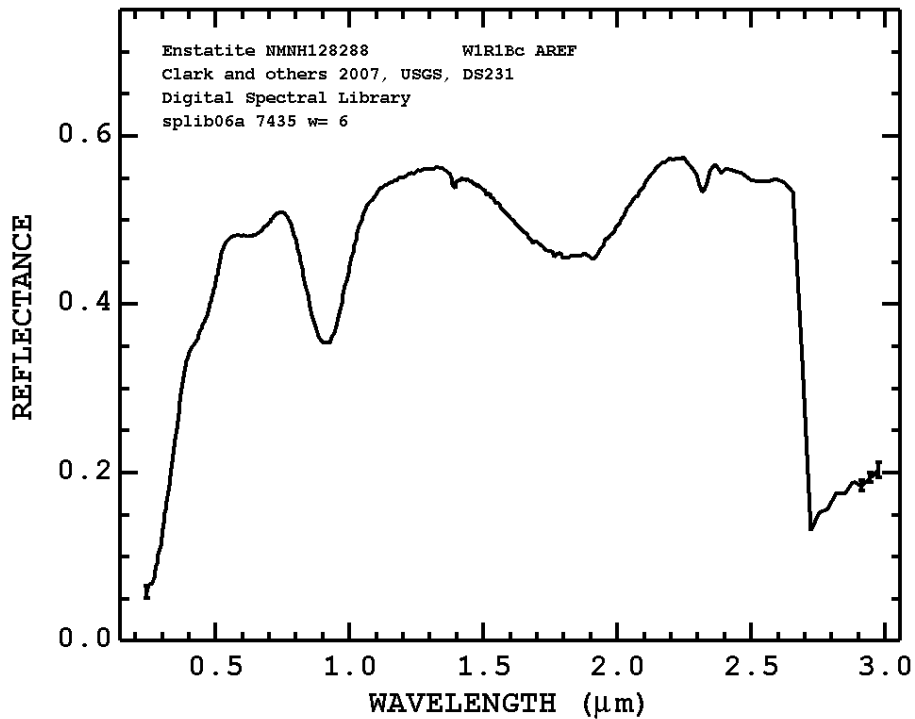


Orthopyroxenes have general formula :



but natural compositions are dominated by two major end member components: enstatite, $Mg_2Si_2O_6$, and ferrosilite, $Fe_2Si_2O_6$.

Low-Ca pyroxene, which may be intermixed with plagioclase shows an absorption band at 890-940 nm while high-Ca pyroxenes have an absorption band toward higher wavelengths (950 nm to 1000 nm).

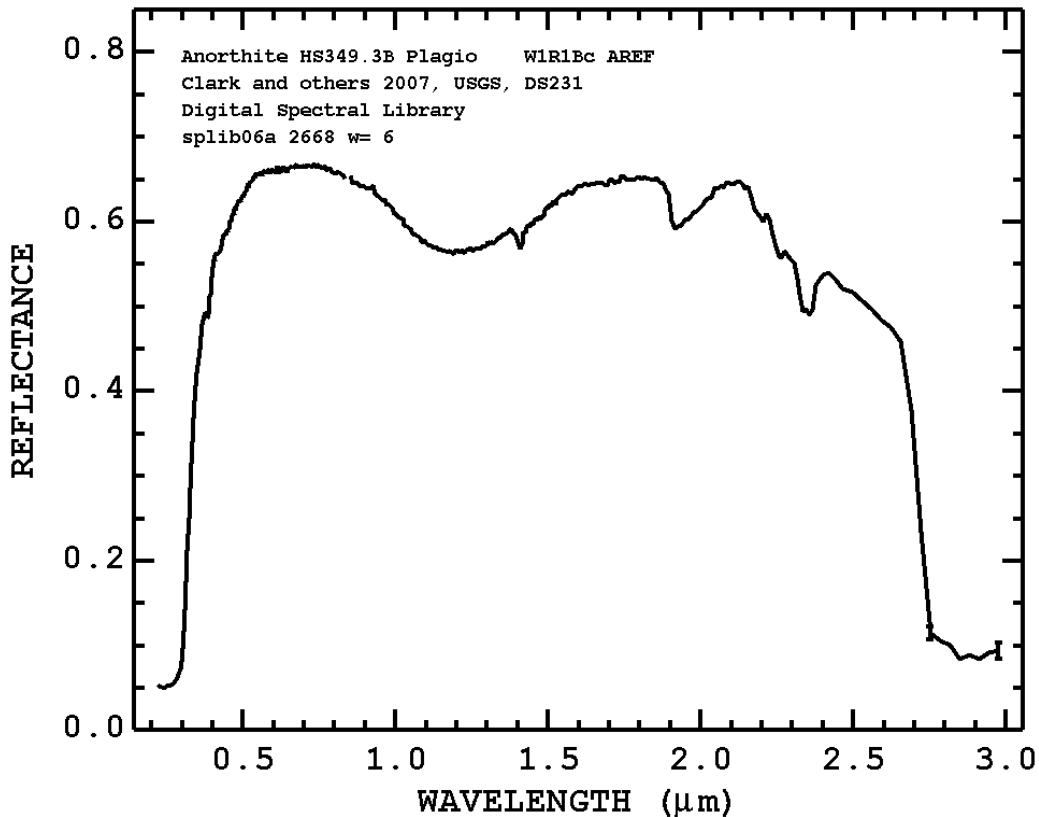


Plagioclase

Plagioclase (a feldspar) is widespread and common in a wide variety of igneous rocks. A highly relevant solid solution is the mineral plagioclase feldspar, the most common mineral in the lunar highlands and in the Earth's crust.

Plagioclase varies from the endmember albite, $\text{NaAlSi}_3\text{O}_8$ to the endmember anorthite, $\text{CaAl}_2\text{Si}_2\text{O}_8$.

Plagioclase feldspar is spectrally characterized by a continuous upward slope from 415 to 900 nm and a broad absorption band at about 1200-1400 nm.

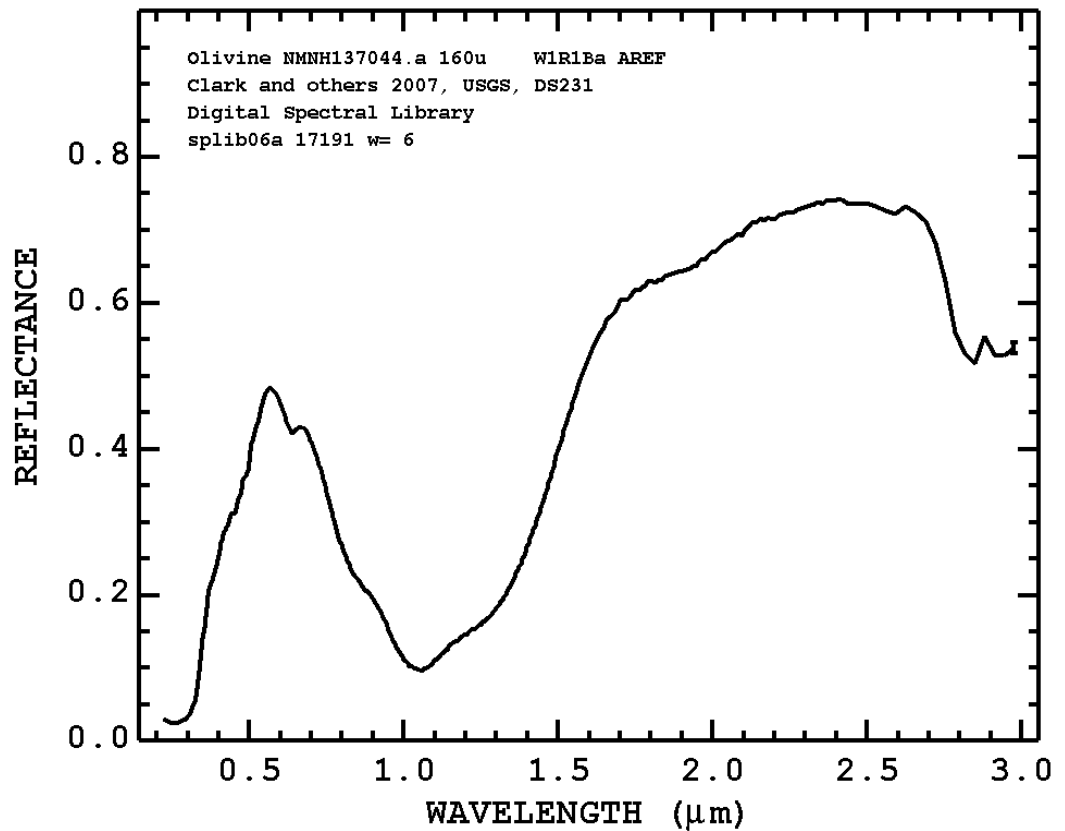


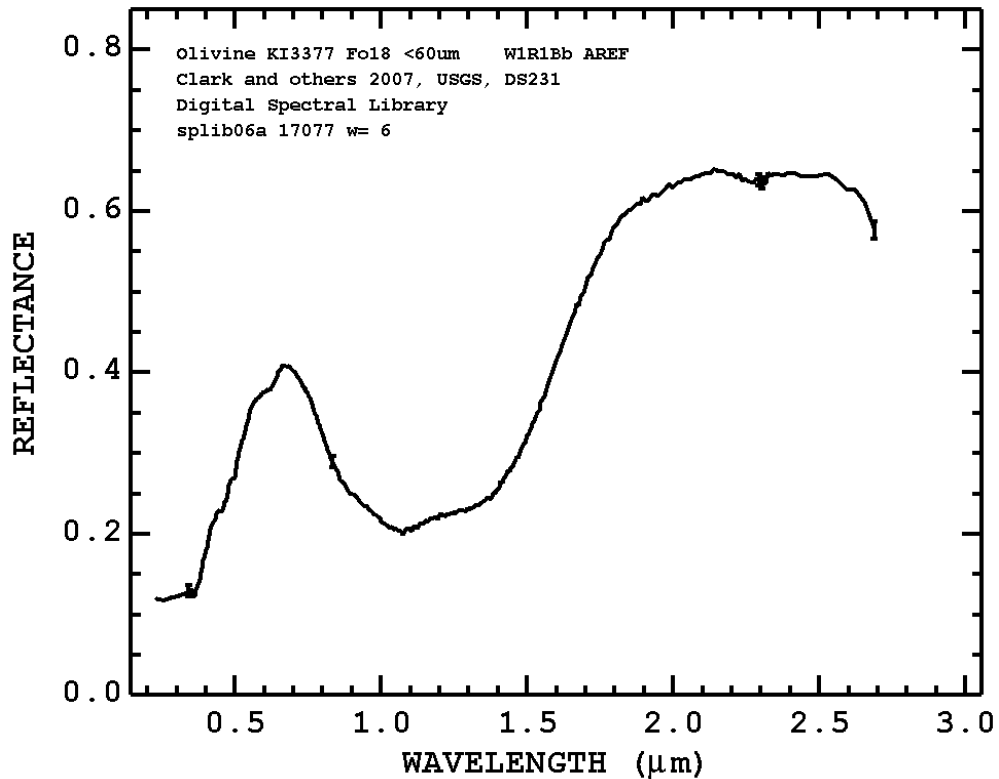
Olivine

The mineral olivine is a common constituent in basaltic rocks on Earth and on the Moon and a minor constituent of the lunar highlands. Olivine chemistry provides an effective illustration of solid solution $(\text{Mg,Fe})_2\text{SiO}_4$. Olivine has a composition between the Mg_2SiO_4 endmember, known as forsterite, and Fe_2SiO_4 , known as fayalite. Magnesium and Fe are both cations of similar ionic radius; thus, they behave similarly in geochemical systems and freely substitute for one another in olivine's crystal lattice (and in other minerals as well). It is common in mineralogy to refer to the composition of a mineral with solid solution by the fraction of one of the endmembers. For instance, pure Mg_2SiO_4 is 100% forsterite, or in common notation, Fo_{100} , and pure fayalite would be Fo_0 .

Olivine has band centers comprised from 1005 to 1100 nm.

Note that pyroxenes absorb at both 1000 nm and 2000 nm but olivine does not absorb at 2000 nm. Plagioclase feldspar shows a broad absorption band at about 1200-1400 nm.





Glass

The term glass refers to a material that solidifies from a molten state. Glass is amorphous and lacks the internal structure that is characteristic of minerals. On the Moon, glass occurs by two mechanisms. One is by meteorite impact. The Moon experienced an early history of cataclysmic bombardment. Another population of lunar glass is composed of volcanic glass. Almost of this material is basaltic (Mg- and Fe-rich), though the contents of other constituents like Titanium vary considerably and result in differences in color (e.g. orange glasses and black beads). The amorphous structure of volcanic glasses of basaltic composition produces broad less well-defined absorption bands centered near 1.0 and 2.0 μm .

Among the various glass types, orange glass can show ultraviolet absorption but typically is associated with a fairly high titanium

content. However if the Mg/Al ratio is < 1.0 the material would not be consistent with a volcanic glass. Most volcanic glasses have Mg/Al ratios in the range of 1.7 to 3.3.

Olivine and certain impact glasses/melts show a band center above $1.0 \mu\text{m}$, but only olivine rich areas will be bright on a $2.0/1.5 \mu\text{m}$ ratio image.

Rocks

A rock is a naturally occurring solid aggregate of consolidated minerals, with or without glass. A rock may contain fragments of other rocks. Igneous rocks are those that form from molten material (magma). Igneous rocks are divided into plutonic and volcanic rocks. Plutonic rocks form when magma is emplaced underground, cools slowly, and crystallizes minerals coarse enough to identify with the naked eye. Volcanic rocks are erupted onto the surface, cool relatively quickly, and are composed of fine-grained minerals and glass. While a large portion of the lunar regolith is composed of free mineral grains and glass particles, there are many identifiable examples of original lunar plutonic and volcanic rocks.

An illustration of the spectral parameters which denote the chemical differences between specific rocks are shown in Table 1.

Rock Type	Mineral	Absorption Band	Remarks
Basalt	High-Ca pyroxene (>50%)	0.95 - 1.00 microns	
Basalt with high olivine	High-Ca pyroxene, olivine (10-20%)	0.95 - 1.00 microns	Olivine broadens absorption band, moves to slightly higher wavelengths
Anorthosite	Plagioclase feldspar, little or no pyroxene (<5%)	No pyroxene absorption band	
Norite	Plagioclase feldspar, low-Ca pyroxene	0.90 - 0.93 microns	Band strength varies with pyroxene content. Pyroxene has higher Ca content, or rock contains component of high-Ca mixed in similar to basalts but have lower abundance of pyroxene.
Norite	Plagioclase feldspar, low-Ca pyroxene	0.93 - 0.95 microns	
Gabbro	High-Ca pyroxene	0.97 - 1.00 microns	Similar to Basalts, but have lower abundance of pyroxene
Gabbro	High-Ca pyroxene with low-Ca pyroxene	0.95 - 0.97 microns	
Dunite	Olivine	1.1 microns	
Troctolite	Feldspar with olivine	1.1 microns	

Table 1

2.1 Primer on Lunar Geology

Ninety-Eight percent of the lunar crust (excluding glasses) is composed of just four minerals: plagioclase feldspar, pyroxene, olivine and ilmenite. The lunar crust appears to have arisen from a stratified global magma ocean in which light weight felsic minerals (plagioclase feldspar) floated on top of the heavier mafic minerals. After solidification of the crust, basin forming impacts fractured the crust and caused an outpouring of mafic basalts into what would become the lunar maria. The lunar highlands were composed of 70-99% plagioclase feldspar with by far the most common mineral being Anorthosite (plagioclase feldspar). Crater impacts caused deeper crust minerals to rebound to the surface at central peaks and crater rims. Minerals present in these features often contain mixtures of plagioclase feldspar and mafic components (Pieters and Englert, 1993; Tompkins, 1998). Examples include Noritic anorthosite, Anorthositic gabbro, Troctolitic anorthosite, Norite, Gabbro, Troctolite, and Dunite. All of these contain plagioclase feldspar but they are differentiated by their mafic components. Norite contains orthopyroxene (low in calcium). Gabbro contains clinopyroxene (higher in calcium). Troctolite contains some olivine while dunite is composed primarily of olivine.

The lunar maria are composed of heavier and darker basalts rich in such mafic components as pyroxenes (with clinopyroxene predominating in the maria while orthopyroxene predominates in highland mafic rocks), olivine and ilmenite (FeTiO_3). Basalts can be classified as low titanium, high titanium and iron rich. High titanium basalts were deposited between 3.85 and 3.55 billion years ago while low titanium basalts were deposited 3.45 to 3.15 billion years ago.

Constructional volcanic features formed during the later stages of volcanism on the Moon, characterised by a decreasing rate of lava extrusion and comparably low temperature of eruption, resulting in the formation of effusive domes. Early stage lavas were very fluid due to

their high temperatures, massive volumes, and mineralogy. Lunar lavas are mafic in composition (low silica content, high metal oxide content) and tend to have a low viscosity, as opposed to felsic lavas (high silica content), from andesite to rhyolite in composition, which on Earth produce steep-sided domes with short lava flows. Early works by Baldwin (1963) and Fielder (1965) have drawn attention to the similarities of lunar domes to terrestrial igneous and volcanic features. The first lavas on the moon flowed from eruptive fissures and did not produce volcanoes. Across time, the erupting lavas cooled, decreased in flow rate, and began to crystallise so that they began to pile up around the vent through which they effused, forming low shield-like volcanoes. Lower effusion rates due to lower speed of lava uplift and magmatic differentiation may have increased lava viscosity, eventually leading to steeper flank slopes. At that stage, extrusion rates were apparently relatively low, compared to the very high values characteristic for flows associated with major lunar sinuous rilles and terrestrial flood basalts, but may have been relatively high compared to similar terrestrial shields. Many of the lunar effusive domes have a central crater pit, which occurs upon magma withdrawal and subsequent collapse into the vent.

The vast majority of domes are in the maria, as this is the place where lunar lavas tracked up deep-seated faults created by the basin impacts. However, a few occur in highland regions, as a variety of 'cryptomare' (lavas covered over by thin veneers of highland material) do occur.

Mare domes differ from distinctive high-albedo domes of volcanic origin located in or near the highlands. The classical examples of highland domes are the Gruithuisen domes, which have a higher albedo than the nearby Mare Imbrium and also larger diameters and steeper slopes than mare domes. This refers to an early volcanism which was

probably unrelated to the lunar maria and was also of different mineralogy (Chevrel et al., 1999). The higher reflectance and spectrally red appearance of these domes supports the assumption of a different mineralogy, which is consistent with lava having a lower FeO and TiO₂ content than mare basalts. It is suggested that the source of this lava is the lower crust, differing from the mare source region, the upper mantle.

Volcanic eruptions created lava flows, domes and pyroclastic deposits on the Moon. More than 100 lunar pyroclastic deposits have been recognized and classified as small and regional deposits on the basis of size and morphology (Gaddis et al., 2003 and references therein). Characterization of the nature of the lunar pyroclastic deposits (LPDs) is essential for models of formation, segregation and emplacement of lunar magmas. There are two styles of volcanism that might leave dark mantling units on the Moon. Regional deposits are thought to have been emplaced as products of continuous or Strombolian-style eruptions, with wide dispersion of well-sorted pyroclasts (Gaddis et al., 2003). Intermittent or Vulcanian-style eruptions likely have produced the small pyroclastic deposits, with explosive removal of a plug of lava within a conduit and forming an endogenic vent (Head and Wilson, 1979; Weitz and Head, 1999). Thus the Strombolian eruptions may have formed the largest dark mantle deposits on the Moon while the Vulcanian eruptions feature short explosions of gas and rocks and tend to be smaller than Strombolian eruptions. Because gases need to build up near the vent, they do not involve large volumes of magma. Hence, Vulcanian eruptions likely form the smaller patches of dark materials on the moon, with a recognizable central pit or vent structure (Head and Wilson, 1979). Among the largest of the dark mantle deposits are Aristarchus plateau, Mare Humorum, South Mare Vaporum and Sulpicius Gallus deposits. The explosive eruptions that formed the lunar dark mantle deposits have been likened to some types of

terrestrial volcanic activity. Intermittently explosive or Vulcanian-style eruptions are likely to have produced the small pyroclastic deposits, with explosive decompression acting to remove a plug of lava within a conduit and to form an endogenic vent crater (Head and Wilson, 1979). The small pyroclastic deposits have been further subdivided into three compositional classes on the basis of their 1.0-micron or mafic absorption bands in Earth-based spectra (e.g., Gaddis et al, 2003). Mafic bands of small pyroclastic deposits in the Group 1 class are centered near 0.93 to 0.95 microns, have depths of 4 to 5%, and are asymmetrical. Their spectra resemble those of typical highlands and are indicative of the presence of feldspar-bearing mafic assemblages which are dominated by orthopyroxene (e.g . small pyroclastic deposits are found on the floors of Atlas Crater). Mafic bands in spectra for Group 2 deposits are centered near 0.96 microns, have depths of ~7%, and are symmetrical in shape. Group 2 spectra are similar to those of mature mare deposits, and they are dominated by clinopyroxene (e.g . two small deposits east of Aristoteles Crater). Small pyroclastic deposits in Group 2 appear to consist largely of fragmented plug rock material, with insignificant amounts of highland and juvenile materials (e.g., Gaddis et al., 2003). Group 3 mafic bands are centered near 1.0 micron, have depths of ~5 to 7%, are relatively broad and asymmetrical, and are probably multiple bands. Spectra of Group 3 deposits are dominated by olivine and orthopyroxene; Examples of Group 3 small pyroclastic deposits are those of J. Herschel Crater (62°N, 42°W) and the well known Alphonsus Crater.

On the other hand, in a Strombolian eruption explosive decompression occurs as the pressure is released and the magma and gas rise in an expanding column of erupting material. For the Moon the particles will spread out over an area roughly six times larger on the Moon than they would for a similar eruption on Earth. Larger fragments will be deposited closest to the vent. A Strombolian eruption is consistent with

the volatile coated spheres returned from the Apollo 17 landing site. Among the largest of the dark mantle deposits are Aristarchus plateau, Mare Humorum, South Mare Vaporum and Sulpicius Gallus deposits. In composite ratio images based on 415, 750 and 1000 nm, the iron rich basalts have a strong absorption signal at 1000 nm and appear greenish. Low titanium basalts appear purplish blue while high titanium basalts like ilmenite basalts appear lighter blue due to titanium absorption at 415 nm. Titanium rich areas of the mare appear more blue and titanium poor areas appear more red in maturation ratio images. These mafic components are mixed with plagioclase. They can be subtyped as being rich or poor in calcium, titanium and aluminum. Ilmenite (FeTiO_3) contains iron but is rich in a titanium oxide. Older lunar features such as the lunar highlands have been exposed to micrometeorite bombardment for eons and have what is termed a “mature” surface soil containing glasses. This mature soil produces the distinctive red appearance on ratio images taken at 415, 750 and 1000 nm as described above.

Dark mantling material (DMD) containing glasses can be recognized using a different combined ratio images. The 750/415 nm ratio image is assigned to the red channel. The 750/950 nm ratio image is assigned to the green channel and the 750 nm ratio image is assigned to the blue channel. Features that have a high 750/415 nm ratio are bright red in color and indicate mature highland soil or glasses (impact or volcanic). A high 750/950 nm ratio produces a green color and indicates the presence of Fe-bearing material, which is referred as a mafic signature. DMDs are low in albedo and therefore have low signal in the 750 nm wavelength region which is represented by the blue channel. In the combined ratio images the dark mantling material appears strongly bright orange or reddish.

>3. Preparation and Significance of Ratio Images

The Clementine probe took a series of lunar images between February and May of 1994. Of the several cameras used, the UVVIS camera provided image sets at 415, 750, 900, 950 and 1000 nm that are particularly useful in the creation of false color and ratio images of geologic significance.

Raw Clementine data is available from the National Space Science Data Center (see http://nssdc.gsfc.nasa.gov/nssdc/obtaining_data.html) in the form of a set of CD-ROM disks. The disks archive the raw UVVIS images by lunar orbital revolution number, the imaging wavelength and the lunar longitude and latitude of the feature imaged. Images are stored in a compressed format and are converted to tif format using a DOS utility program (clemdcmp.exe) which is provided. Creation of false color images by assignment of a single wavelength to a particular color channel can provide some useful geologic information about the iron and titanium content of the surface (Flor et al., 2003; Gillis et al., 2004; Giguere et al., 2000). Iron preferentially absorbs at 1000 nm while titanium absorbs at 415 nm (Lucey et al., 1998; Lucey et al., 1995). However, it is usually more informative to assign ratio images to color channels since this has the effect of reducing the effects of albedo. These images are created by dividing an image taken at one wavelength by a second co-registered image taken at different wavelength. Assigning different ratio images to the red, green and blue color channels of a single image produces a single combined ratio image.

Combined ratio images created from an image set taken at 415, 750 and 1000 nm provides basic information on lunar surface maturation and limited information about mafic composition (Tompkins et al., 2000); Spudis et al., NASA publ). The 750/415 nm ratio image is assigned to the red channel. The 750/1000 nm ratio image is assigned to the green channel and the 415/750 nm ratio image is assigned to the blue

channel. We will refer to this composite ratio image as a **maturation ratio image**. When the RGB image is viewed, mature highland soils appear red or orange due to the high glass content that results from eons of micrometeorite bombardment. Surfaces low in titanium content also have a reddish color and pyroclastic orange glass deposits have a very deep red color (Gaddis et al., 2003). Freshly excavated lunar features appear blue as do mare surfaces having a high titanium content (ilmenite rich). Mafic components, typically rich in iron, absorb at 1000 nm and appear yellowish green (due to mixture of the reddish orange of mature soil with the green characteristic of mafic absorption) or deep indigo blue (titanium poor basalt). Mature mare soils appear reddish or purplish while freshly exposed mare surfaces appear yellowish. The basalts of the maria give the strongest signals, but weaker mafic components in certain highland features can also give a response. Yellow color signals often indicate freshly excavated basalt features, especially when found in crater and rille walls. Bright blue signals indicate a freshly exposed non-mafic terrain (i.e. such as freshly exposed Anorthosite).

Combined image ratios created from 415, 900, 950 and 1000 nm images provide additional information on surface mafic constituents. The usual scheme is to assign 750/900 nm to the red channel, 750/1000 nm to the green channel and 750/950 to the blue channel (Tompkins et al., 2000). We will refer to this ratio image scheme as a **mafic ratio image**. Using this scheme low calcium pyroxenes (orthopyroxenes like Norite or Noritic anorthosite) appear reddish, olivines (such as Olivine, Dunite, Troctolitic anorthosite, and Troctolite) appear brighter green, and high calcium pyroxenes (clinopyroxenes like Gabbro or Anorthositic gabbro) appear bright blue. Anorthosite doesn't absorb and appears dim grayish green which can be compared geographically to its blue appearance on ratio images taken at 415, 750 and 1000 nm (see above). This response is useful in subtyping mare basalts and also

for detecting and subtyping the weaker mafic constituents found in pyroxene bearing plagioclase in the lunar highlands. In addition, comparison of an albedo image with a single ratio image taken at 750/1000 nm can assist in differentiating anorthositic features from other high albedo features such as recently formed craters and their ejecta.

The Maturation Ratio Image

False color composites are created by copying each image to a particular channel in a blank color photograph. Typical channel assignments include 1) red=750 nm, green=1000 nm, blue=415 nm; and 2) red=1000 nm green=900 nm, blue=415 nm. The channels are then balanced for brightness and contrast.

Creation of composite ratio images is slightly more complex. The 750 nm image is divided by the 415 nm image using software designed for this purpose. We use a Windows based freeware program, ImageJ (see <http://rsbweb.nih.gov/ij/>). Similarly, the 750 nm image is divided by the 1000 nm image and the 415 nm image is divided by the 750 nm image. This process creates three separate ratio image files: 750/415 nm, 750/1000 nm and 415/750 nm. These files are then respectively assigned to the red, green and blue channels of a blank color image. The channels are then balanced for brightness and contrast.

The Mafic Ratio Image

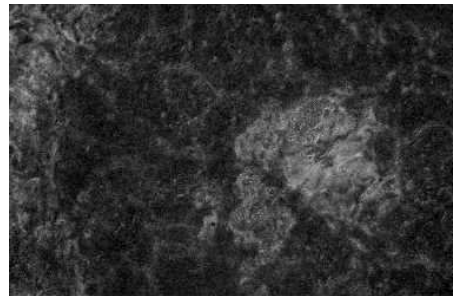
Using the same techniques, a combined ratio image is created in which the channel assignments are: red=750/900 nm, green=750/1000 nm and blue=750/950 nm. Creative individuals can also try combining single wavelength channel assignments with ratio image assignments. One scheme of this nature that is sometimes used has the following channel assignments: red=750 nm, green=950/750 nm, and blue=415/750 nm.

I. Example: False Color and Ratio Image Study of Tycho Central Peaks

Clementine spectral band images can be downloaded from the USGS map a planet lunar website in 16 bit tiff unstretched format and opened in ImageJ. ImageJ (<http://rsbweb.nih.gov/ij/>) allows arithmetic functions to be performed between band images using the Process > Image Calculator menu. Ratio images can be created by dividing one band image by another in this way.



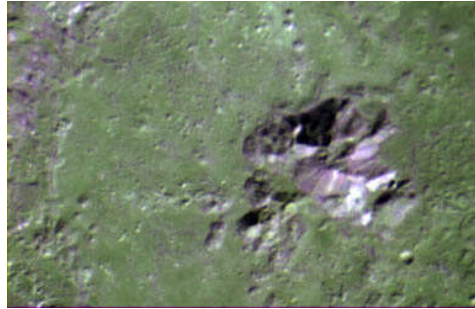
750 nm



750/1000 nm

The images are of good quality and are not over saturated by albedo features. The 750/1000 nm image removes what little albedo problems exist in the 750 nm image. The brighter areas on the 750/1000 nm image have the potential to be mafic materials. The images show enough promise to warrant further processing of the image set.

The next step involves the creation of two false color images. The first was created by assigning 750, 1000, and 415 nm images to red, green and blue color channels. The second was created by assigning 1000, 750 and 415 nm images to red, green and blue color channels.



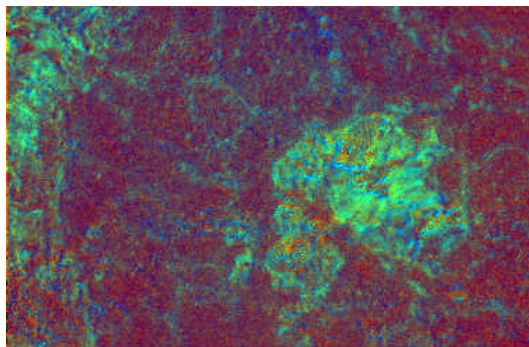
R=750 G=1000 B=415



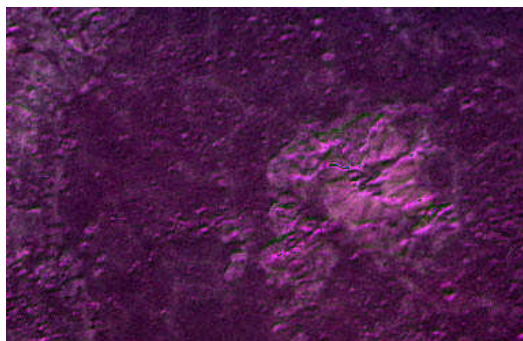
R=1000 G=900 B=415

The images begin to reveal a high likelihood that the central peaks are composed of mafic materials. The peaks are darker than the surrounding crater floor and show subtle compositional variation.

Creation of a “maturation” and a “mafic” composite ratio image proceeds as follows. The maturation image is created by assigning the 750/415, 750/1000, and 750/415 nm images to the red, green and blue channels respectively. The mafic image is created by assigning 750/900, 750/1000, and 750/950 nm images to the red, green and blue channels.



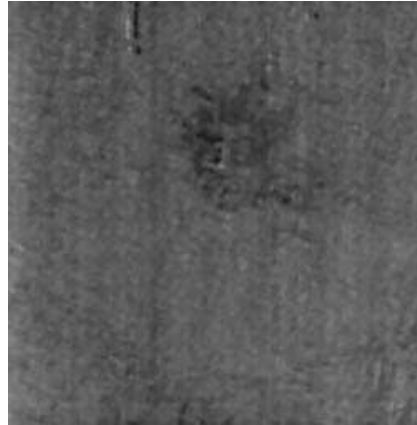
“Maturation” Ratio Image



“Mafic” Ratio Image

The strong green coloration in the maturation image confirms the mafic nature of the central peaks and adjacent crater wall. The floor of the crater consists of mature regolith with a reticulated pattern of mafic material spread on it. Although it has a strong mafic signature, the mafic element composing the central peak is not olivine. If it were present olivine would have a green signature on the mafic ratio image. Rather, the mafic image coloration supports the mafic element being a pyroxene. It is sometimes possible to differentiate high calcium from low calcium pyroxenes. The color signature of the high calcium pyroxenes (clinopyroxenes) is bluish green through bluish violet on a mafic ratio image while the signature of a low calcium pyroxene (orthopyroxene) is distinctly red. On that basis, it appears that the mafic ratio image above would best support a high calcium pyroxene as the principal mafic component. The leading mineral contender would be clinopyroxene which is commonly found in gabbros but can also be present as a minor component in mainly anorthositic rock, or be mixed with other pyroxenes as well.

A single ratio image of 2000 nm/1500 nm has been shown to be very useful in the discrimination between the pyroxenes and olivine. If the feature in question is bright in this ratio image then the presence of olivine is favored. This is because pyroxenes absorb at both 1000 nm and 2000 nm but olivine does not absorb at 2000 nm (cf. section 2).

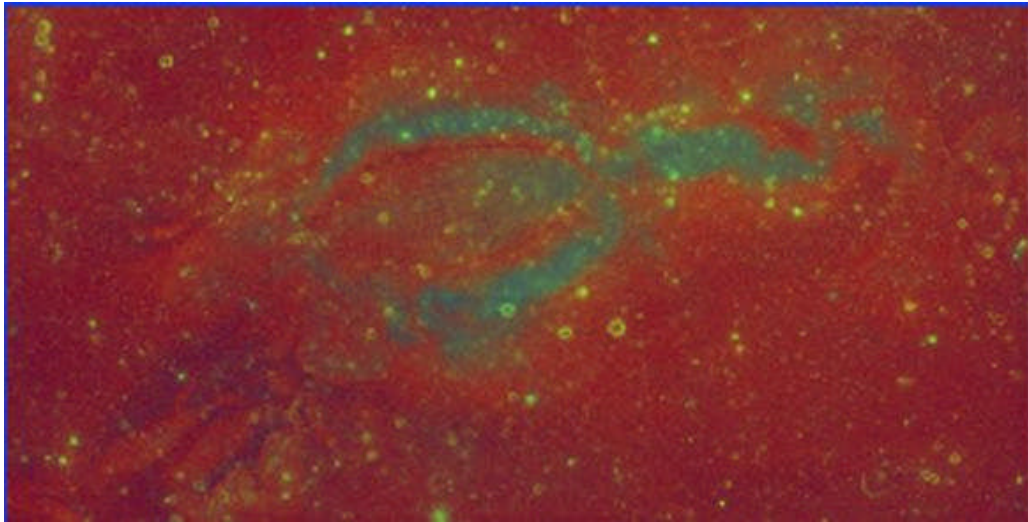


2000/1500 ratio

Since the central peak area is quite dark in the 2000/1500 nm ratio image, there is no indication of the presence of Olivine.

II. Example: False Color and Ratio Image Study of Reiner γ

To create a maturation image of the Reiner γ the 0.750/0.415 μm ratio image is assigned to the red channel, the 0.750/1.000 μm ratio image is assigned to the green channel and the 0.415/0.750 μm ratio image is assigned to the blue channel. In the maturation image immature surfaces appear greenish-blue while older mature soils appear reddish. The yellow color indicates freshly excavated basalt features. Small areas of swirl material to the north and south of the central region of Reiner γ show the same spectral characteristic in a more subdued form. The elliptical dark line inside the swirl appears composed of mature soil that has been exposed to normal lunar weathering processes.

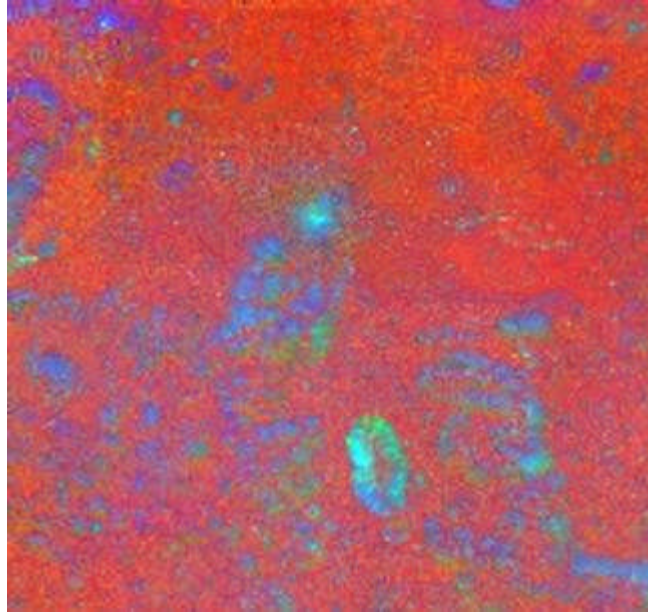


Reiner γ maturation image

III. Example: False Color and Ratio Image Study of Orientale dark mantling material

Dark mantling material (DMD) containing glasses can be recognized using a different combined ratio images. The 750/415 nm ratio image is assigned to the red channel. The 750/950 nm ratio image is assigned to the green channel and the 750 nm ratio image is assigned to the blue channel.

The DMD anular ring shows an evident orange color, while the surrounding highland terrain appears red. The hilly terrain and the elongated vent show a green and a light blue color.



>4. Introduction to Lunar Spectra

Lunar spectra can be obtained from probes orbiting the Moon or from Earth based telescopes (professional or amateur instruments). In either case they can be created from multiple filter images taken at different discrete wavelengths or created as continuous spectra using a slit/grating or objective prism spectroscope. This manual concerns itself with UV-visible-NIR spectra in the range of about 415 nm (i.e. 0.415 micron) through about 2000 nm (2.0 micron). Spectra taken through the Earth's atmosphere will show reduced or absent sensitivity at UV wavelengths and at certain NIR wavelengths due to atmospheric absorption and these effects are worse at sea level. Lunar spectra are typically calibrated against the geography of the Apollo 16 landing site because numerous lunar samples from this area were returned to Earth for spectral study. The sample most often used for calibration of spectra is sample # 62231 and calibration data are available for directional hemispheric reflectance (used to calibrate Earth based telescopes) and bidirectional hemispheric reflectance (used to calibrate probe spectra). Earth based telescopic spectra of a lunar feature can be normalized by

dividing each discrete spectral band image (or a continuous spectral band image from a spectrometer) by its corresponding image of the Apollo 16 landing site taken at approximately the same date and time. The normalized spectra are then calibrated by multiplying them by spectra of lunar soil sample #62231 for corresponding wavelengths.

Clementine probe spectra have already been well calibrated for wavelengths between 415 nm and 2000 nm and can be downloaded from the USGS map a planet website at: <http://www.mapaplanet.org/explorer/moon.html>

Band spectra are downloaded in 16 bit tiff format with no stretch applied. Clementine spectra can be converted to absolute reflectance by multiplying them by 0.000135.

Selene probe spectra have not yet been completely calibrated but the general method used for Earth based telescopes can be employed (but using bidirectional reflectance data).

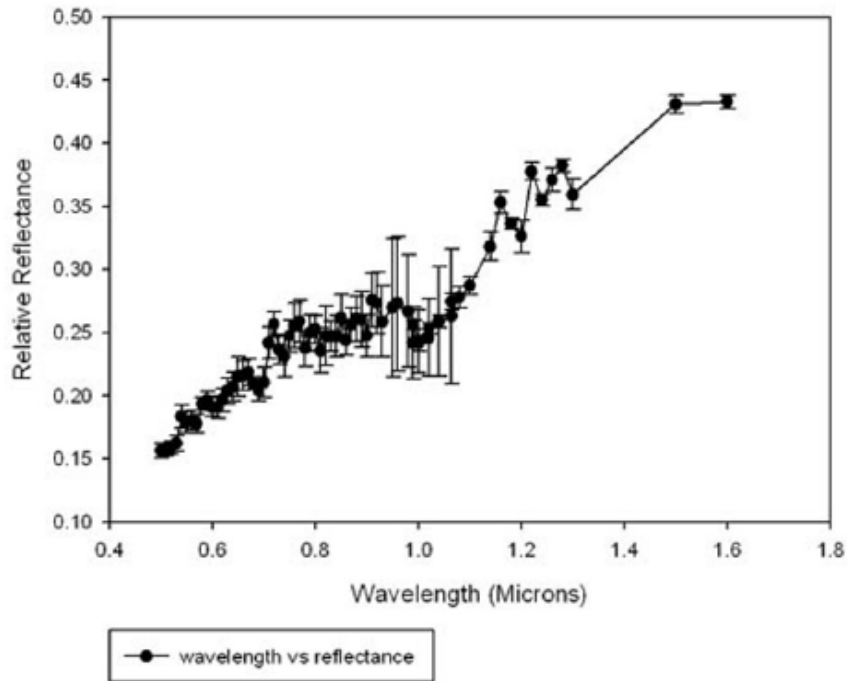
>5. Working with Spectra

We made the spectra below of a basaltic area in the wall of Dionysius crater using a 9.25 inch Schmidt Cassegrain telescope and two cameras (VIS, and NIR) with a series of 50 band filters.

The spectra were obtained near sea level. The spectra were calibrated by division by the Apollo 16 band images and multiplication by lunar soil sample #62231 directional hemispheric reflectance for corresponding wavelengths. Sample #62231 data can be obtained from:

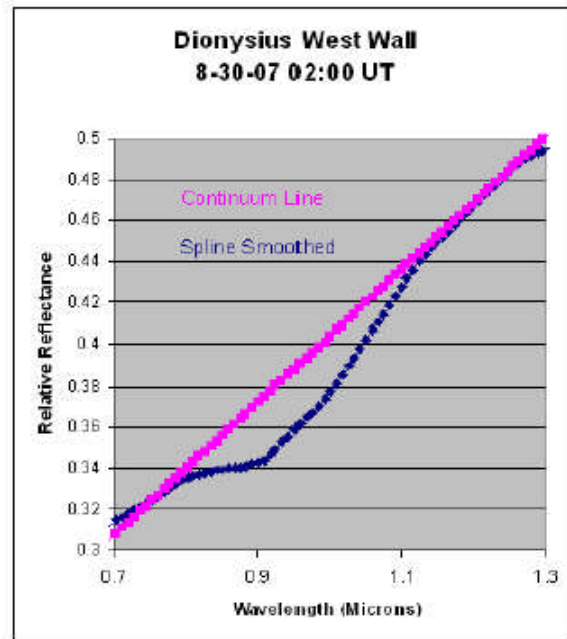
<http://pds-geosciences.wustl.edu/missions/lunarspec/>

Dionysius West Wall
8-30-07 02:00 UT

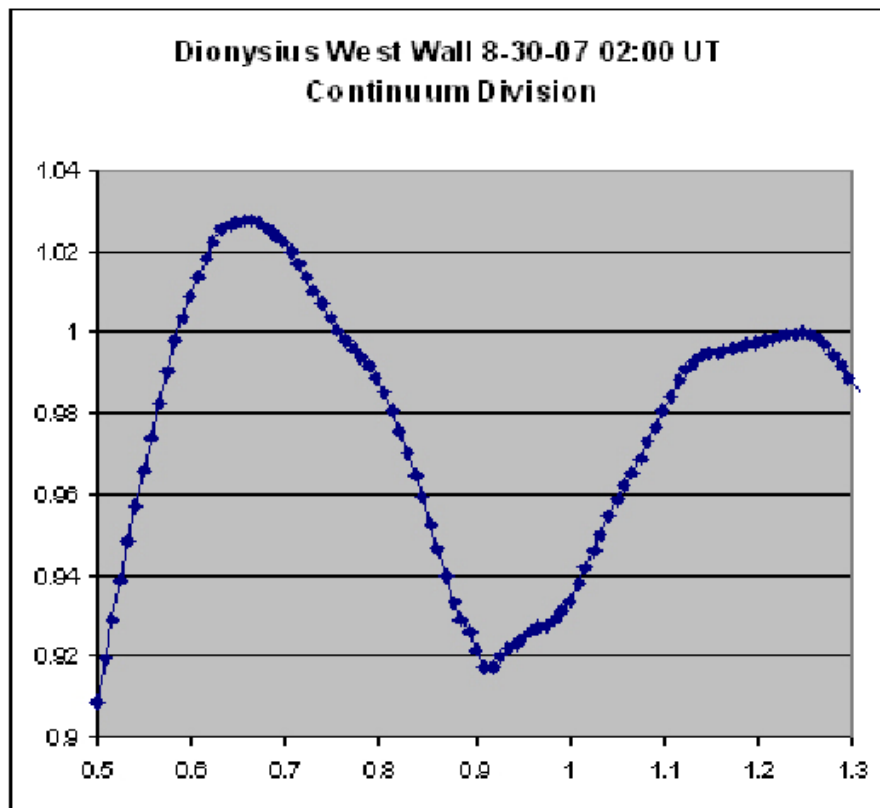


The trough near 1.0 micron is the characteristic iron absorption trough whose parameters (band center, band depth, and FWHM width) are useful in mineral characterization.

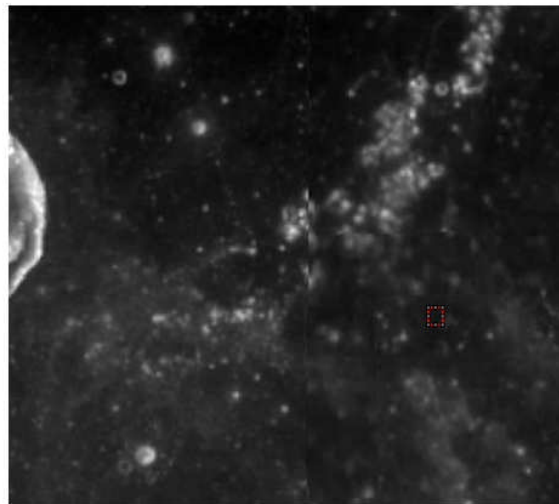
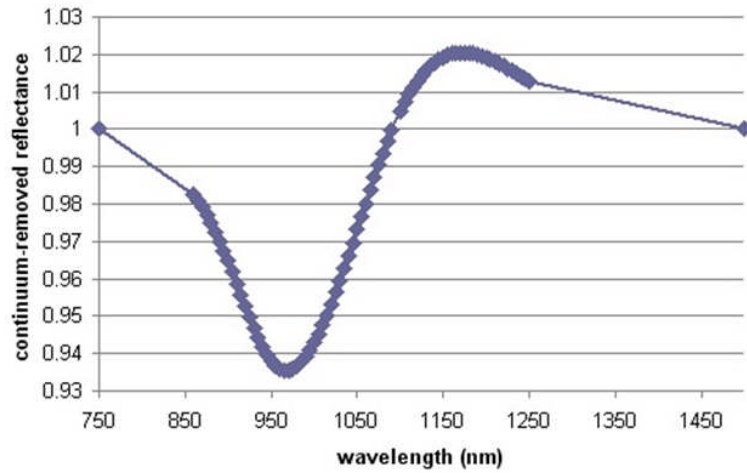
To better visualize this trough a continuum division is performed. To do this, a line is taken connecting the 0.75 and 1.5 micron reflectances on the reflectance vs wavelength curve.



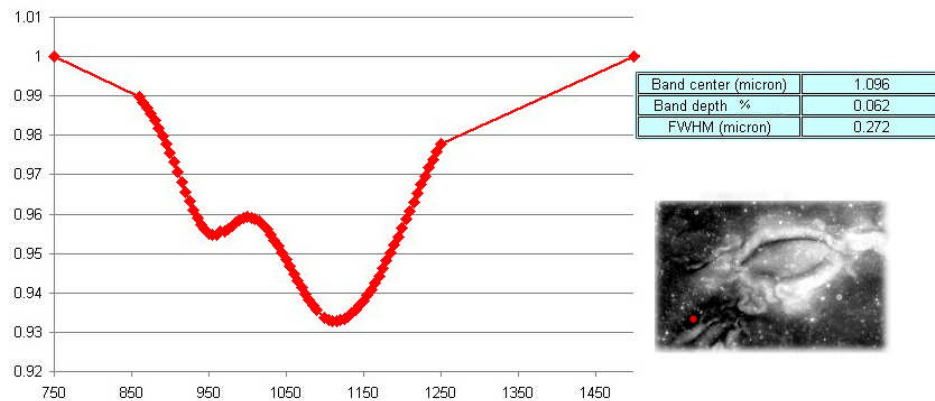
Reflectance values for points along the curve shown above are then divided by the reflectance values of corresponding points along this line. Additional interpolated points can be added to the feature curve before or after continuum division using a cubic spline interpolation. The best spline interpolation of this type is the Akima interpolation (discussed later).



Pyroxenes are common lunar minerals showing this absorption trough. Low calcium pyroxenes (orthopyroxenes) such as norites have a band center between about 0.89 and 0.94 microns. Higher calcium pyroxenes (clinopyroxenes) such as gabbro have a band center between about 0.95 and 1.0 micron. Mixtures have band centers in between. Olivine and certain impact glasses/melts show a band center above 1.0 micron, but only olivine rich areas will be bright on a 2.0/1.5 micron ratio image. In the image below, an individual Clementine spectral plot for the marked region near Flamsteed P, an absorption band at 0.97 micron is due to the presence of a clinopyroxene.



As shown in the following figure, the surface west of Reiner γ is characterized by a shallow pyroxene absorption at 0.950 μm and a second deeper absorption at 1.096 μm which is due to an admixed olivine component in the basaltic lavas.



Band depth is usually (but not always) proportional to mafic character (i.e. a greater concentration of iron bearing minerals). This relationship is not necessarily valid in areas where lunar prospector GRS (gamma ray spectrometer) elemental abundance maps for iron are anomalous with regard to Clementine spectral iron estimates. Lunar areas with less than about a 5 percent mafic content are not very mafic and can range from nearly pure anorthosite (the primary constituent of the primitive lunar crust) to impure anorthosite containing small amounts of iron bearing minerals. Titanium rich areas (typically ilmenite rich mare areas) may show an additional absorption at between 0.43 and 0.45 nm. So, basic inspection of the band center, depth and FWHM of the absorption trough near 1.0 micron can give information about mineral content. However, more definitive information requires determination of elemental abundances for Fe, Mg, Ca, Al, Ti, and O. One then uses the amount of each of these present in wt% to determine lunar mineral content and/or rock composition.

>6. Clementine Five Band UVVIS Spectra

Tompkins and Pieters (1999) showed that the shape of Clementine five band UVVIS Spectra (0.415 to 1.00 microns) correlates with the mineral content of lunar features.

We have applied this type of analysis to the crater Brayley below.

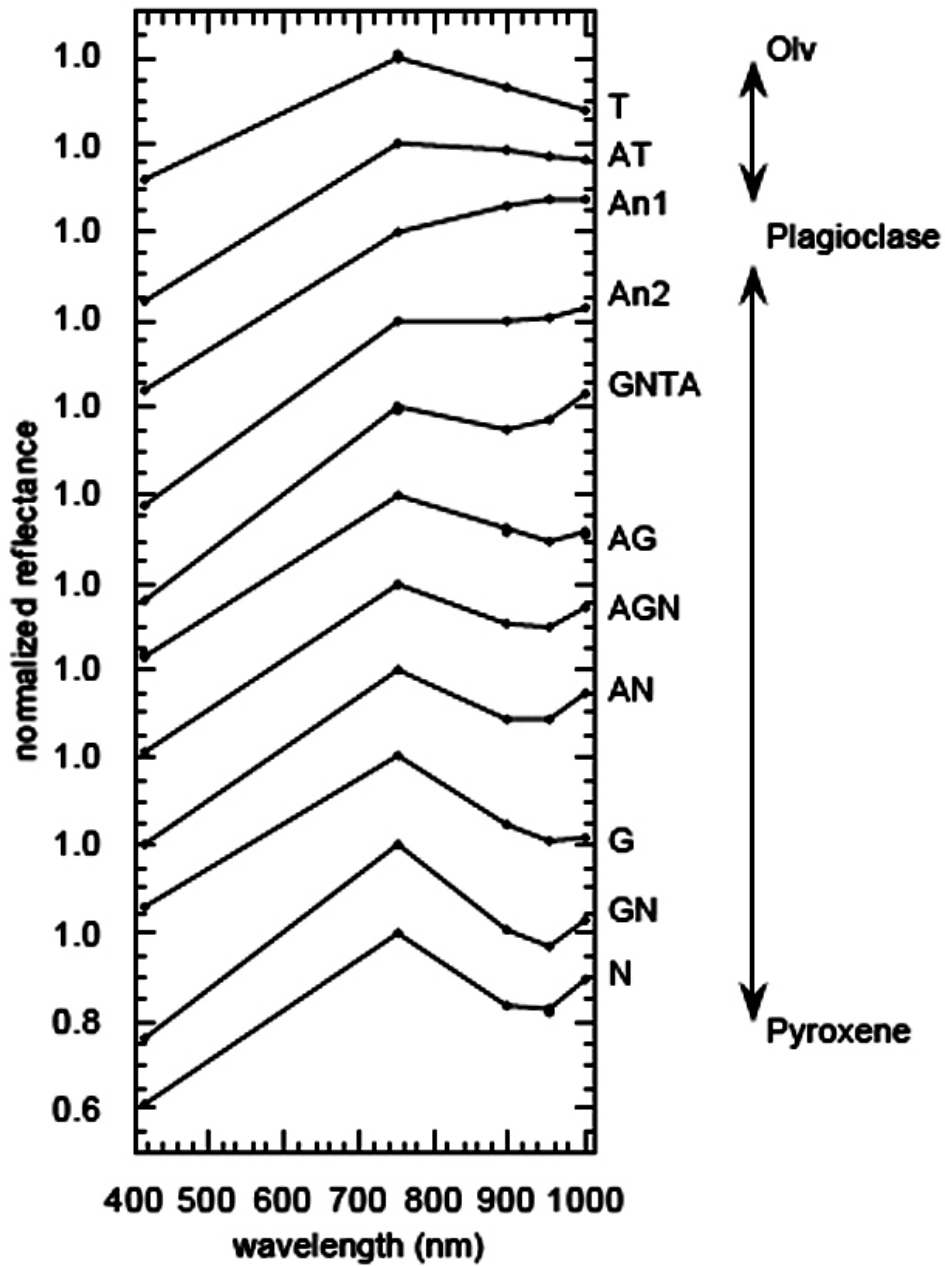
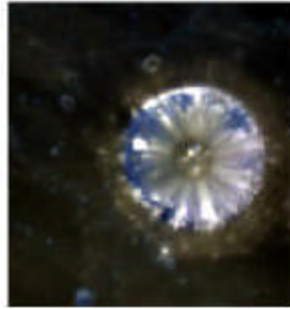


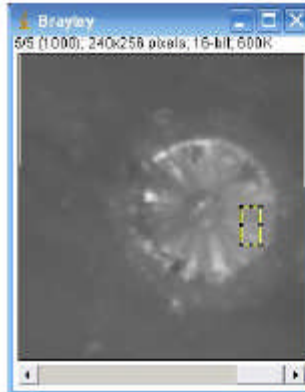
Figure reproduced from (Tompkins, 1997) with the kind permission of Dr. Stephanie Tompkins.



Natural Color



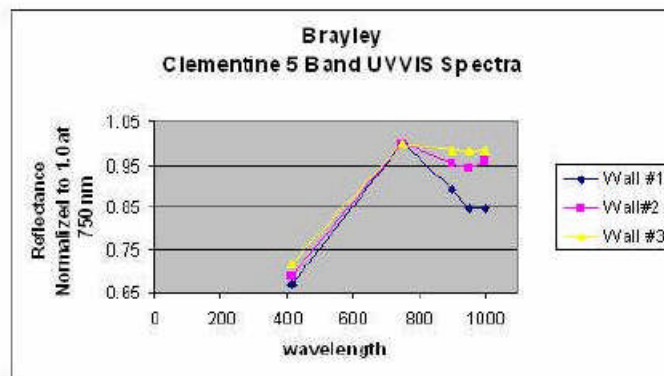
Wall Area #1 (box)



Wall Area #2 (box)

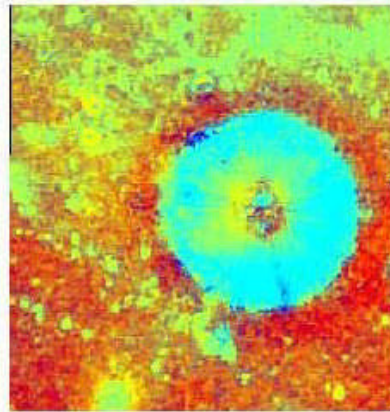


Wall Area #3 (box)





Natural Color



Maturation Ratio

Note that the spectra are normalized to 1.0 relative reflectance at 0.75 microns. The five band UVVIS spectral shape indicates that much of the crater is anorthosite type 2 (An2) but that the darker areas contain anorthositic gabbro, likely from mixture with mare basalt contamination.

>7. Alternate Calibrations of Clementine UVVIS+NIR Imagery

The Clementine NIR camera had some problems with thermal instability that can affect the 1, 1.1 and 1.25 micron imagery in particular and producing a greater error than is acceptable. This, and also differences in slope between Clementine and Earth based telescope results have led to the development of alternate calibrations to the standard USGS based calibration. These alternate calibrations, however, are still based on Apollo 16 site and soil sample #62231. Two alternate calibrations are listed here and consist of a series of gain and offset values for each Clementine band image (i.e. the appropriate band image is multiplied by the gain and then the offset is added to the image). These are the Lucey calibration and a calibration developed by GLR which makes use of spectral data from the 2.2 meter Mauna Kea telescope available on the internet. Both calibrations were developed

using a linear regression technique of Earth based telescopic vs Clementine results for a number of lunar features. The GLR calibration is termed a “Keck” calibration because the 2.2 meter telescope is now affiliated with the Keck observatory. The gain and offset values in the tables below are applicable to all lunar features and do not need to be re-calculated on a case by case basis.

Lucey Aristarchus Plateau Gain and Offset Calibration:

Band	Gain	Offset
0.415	1	0
0.75	1	0
0.9	1.012	-0.0004
0.95	1.036	-0.0008
1.0	1.056	-0.002
1.1	0.87	0.246
1.25	0.854	0.316
1.5	0.792	0.0514
2	0.742	0.0680

Note: The Clementine UVVIS+NIR spectral value for each band is multiplied by the gain and the offset is added to the result

Keck 8 crater peak calibration:(must be applied only to continuum divided spectra)

Band	Keck 8 Peak Calib. Gain	Keck 8 Peak Calib. Offset
.75 micron	1	0
.9 micron	0.652077	0.334652
.95 micron	0.73328	0.25725
1.0 micron	0.658683	0.330151
1.1 micron	0.787658	0.206805
1.25 micron	0.6115316	0.385579
1.5 micron	1	0
2.0 micron	0.263676	0.697133

>8. FeO and TiO₂ Estimation Using Clementine Band Images

There are two ways to estimate iron or titanium content. The first is to use spectral parameters to directly estimate FeO and TiO₂ content, but

this method has the problem of some albedo sensitivity and some error on this basis (especially for TiO₂). Equations have been developed by Lucey and LeMouelic (and others) to estimate FeO and TiO₂ from Clementine band images.

(Eq. 1) Continuum Slope Determination

$$\text{slope} = (1/R_{750}) * (R_{1500} - R_{750}) / (1.5 - 0.75) \text{ abs. refl./micron}$$

This slope value is scaled to tangency at 0.75 microns

(Eq.2) Trough Depth Uncorrected for Continuum Slope

$$\text{depth}_1 = 1 - [(R_{950}) / ((2.2/3)R_{750} + (0.8/3)R_{1500})]$$

(Eq. 3) Trough Depth Corrected for Continuum Slope

$$\text{FeO}_{\text{mafic}} = \text{depth}_1 + 0.286 * \text{slope}$$

The slope calculated in Eq. 1 was scaled to tangency at 0.75 microns

(Eq. 4) Titanium Oxide content in wt. %

$$\text{TiO}_2 = (\theta_{\text{Ti}}^2 * 20.79) - ((\theta_{\text{Ti}} * 22.928) + 5.909)$$

(Eq. 4a) where: $\theta_{\text{Ti}} = \arctan [((R_{415}/R_{750}) - 0.45) / (R_{750} - 0.05)]$

and: R_{750} is in absolute reflectance (i.e. $R_{750} * 0.000135$)

(Eq. 5) Total Iron content in wt. %

$$\text{total FeO} = 45.6(\text{depth}_1 + 0.286 * \text{slope}) - 3.8 + 0.9 \text{ TiO}_2$$

Here, for example is an FeO wt% map of Alphonsus crater based on this approach where the three pyroclastic rich deposit areas are seen to be bright (i.e. have a high FeO content). The central peak of Alphonsus is less mafic and more anorthositic and is the small dark focus in the midst of the three pyroclastic areas.



Another important concept is the OMAT (Optical Maturity) map in which brighter pixels represent younger features and darker features represent older features that have been long subjected to lunar weathering processes. There are several possible equations for the calculation of the OMAT map, but one of the more common variants is listed below:

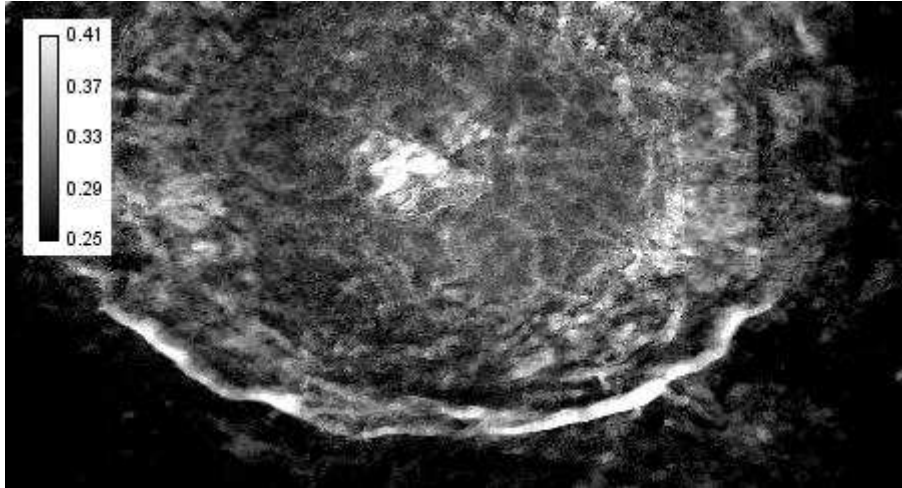
$$\text{OMAT} = \text{sqrt} [(R_{750} - 0.08)^2 + (R_{950}/R_{750} - 1.19)^2]$$

where R denotes the calibrated Clementine band image in absolute reflectance (i.e. multiplied by 0.000135).

Another variant is to replace the 0.08 and 1.19 coefficients with 0.04 and 1.22. Still another variant developed by Wilcox in 2005 is:

$$\text{OMAT} = (R_{750} * 0.1813) - (R_{950}/R_{750}) * 0.9834$$

An OMAT map of Tycho crater is shown in the following figure.



Octave code for producing an OMAT map using the Lucey 2000 equation:

OMAT = $\sqrt{[(R_{750} - 0.08)^2 + (R_{950}/R_{750} - 1.19)^2]}$ is shown below:

% creates an omat map from a 750 and 950 nm band image in the same directory

```
d2=dlmread("750.txt");
e1=dlmread("950.txt");
e2 = (d2.*.000135 - .08).^2;
e3 = ((e1./d2) - 1.19).^2;
e = (e2 + e3).^0.5;
% save OMAT as matrix 013
filename = sprintf('matrix%03d.mat',13);
save(filename,'e')
```

Just as there are variant estimations for the OMAT, there are also variant estimations for FeO and TiO₂.

Estimations developed by Lucey in 2000 are listed below:

$$\text{FeO} = 17.427 \text{ Theta}_{\text{Fe}} - 7.565$$

where $\Theta_{Fe} = -\text{atan2} [((R_{950}/R_{750}) - 1.19) / (R_{750} - 0.08)]$
and reflectances are in absolute reflectance as described above.

$$\text{TiO}_2 = 3.708 \Theta_{Ti}^{5.979}$$

where $\Theta_{Ti} = \text{atan} [(R_{415}/R_{750}) - 0.42 / R_{750}]$

Before we suggest a better method for evaluating elemental abundances (i.e. which is much less albedo sensitive), it is first necessary to define an automated method of achieving maps of the basic spectral parameters: band center, depth, FWHM and slope of the principal absorption trough near 1.0 micron.

>9. Spectral Parameter Mapping in Octave

GLR has developed an Octave m file program, ClementineMaps.m, which produces spectral maps of the basic spectral parameters: band center, depth, FWHM and slope of the principal absorption trough near 1.0 micron. Octave can be downloaded from here:

<http://www.gnu.org/software/octave/>

The Octave m program codes are listed in Appendix 1.

The program requires to additional m files (akima.m and fwhm.m) to function. These three m files and also the Clementine band images from 0.75 to 1.5 micron must be present in the same directory for ClementineMaps.m to function. Although these band images are downloaded in 16 bit non-stretched tiff format from the map-a-planet website, they must be converted to .txt format using ImageJ to work using this Octave application. ImageJ (version 1.43r is suggested) can be downloaded from: <http://rsbweb.nih.gov/ij/>. Typically an earlier version is downloaded and then upgraded as per the instructions. Knowledge of the basic operation of this program is needed for many lunar spectral activities undertaken by GLR. Basically, in this case the

tif images are opened and saved as text images.

Running ClementineMaps.m

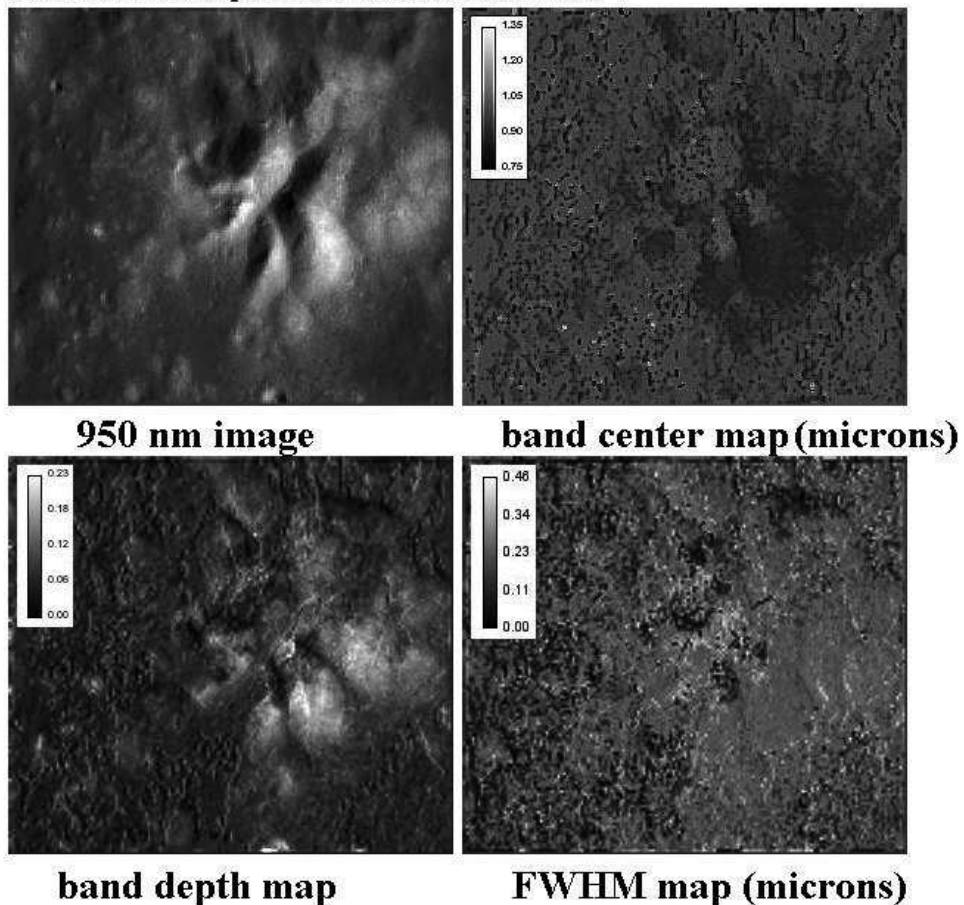
The program is run in Octave from the directory in which it, `akima.m`, `fwhm.m` and all Clementine band maps in txt format are located. The band maps must be named as follows: `750.txt`, `900.txt`, `950.txt`, `1000.txt`, `1100.txt`, `1250.txt` and `1500.txt`. `Akima.m` is used to create a cubic spline interpolation used by `ClementineMaps.m` and `fwhm.m` is used to create the full width at half maximum value for each map pixel. To run `ClementineMaps.m`, simply type `ClementineMaps` from the prompt, provided that this is done from within the correct directory in which all of the above files are located. A basic knowledge of Octave is essential to GLR activity in spectral work.

Running the program successfully produces three spectral parameter maps within the same directory as the other files discussed above. Program run time depends on the image size and is about 2 hours for small images and about 24 hours for large images. These are `bandcenter`, `banddepth`, and `fwhm`. Each of these files is in a text format with header information. To remove the header information each of these files is opened in Open Office Calc (or Excel 2007) and the files re-saved as CSV files (Open Office Calc) or MS-DOS txt files (Excel 2007). In Open Office Calc, the files will then have a `.csv` extension. Either file type can then be opened in ImageJ and saved as nearly any desired file type, which for input into other GLR Octave programs is a `.txt` format. To open `bandcenter`, `banddepth`, or `fwhm` in Open Office Calc, use the Insert > sheet from file selection. A basic working knowledge of Open Office Calc and/or Excel 2007 is basic to GLR spectral work. For use in other GLR Octave programs such as `applycoeff.m`, it is necessary to convert `bandcenter.csv`, `banddepth.csv` and `fwhm.csv` to `.txt` format using ImageJ version 1.43r or later.

Spectral maps produced for Bullialdus central peak area are shown below. They have been converted to jpg format and a calibration bar inserted using ImageJ.

**Bullialdus Peaks - Selene VIS+NIR Imagery
Keck Calibration. Maps made in Octave.**

Keck 120 color spectra calibration file HB0974



Examination of spectral maps prepared using the Clementine UVVIS+NIR dataset reveals that the region of Flamsteed is composed almost exclusively of clinopyroxene bearing rock with a band center near $0.970 \mu\text{m}$, a band depth of 0.08 and a FWHM width of $0.18 \mu\text{m}$. There is some indication of the presence of orthopyroxene and olivine

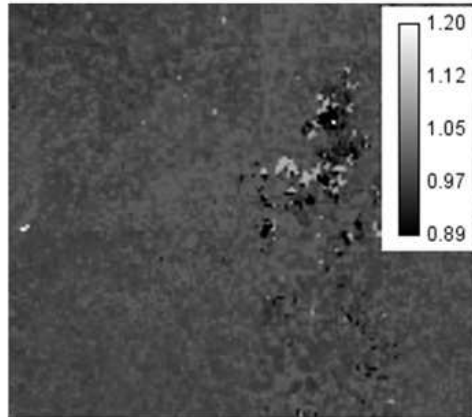
on the wall of the ruined ring formation known as Flamsteed P. The olivine signature rather than impact melt is identified by the olivine band center and depth maps and is confirmed by the 2.00/1.50 ratio which shows the same regions as being bright.

The segregated maps corresponding for orthopyroxene band center (0.890 to 0.945 μm), clinopyroxene band center (0.950 to 1.000 μm), and olivine band centers (1.005 to 1.095 μm), are used to derive a false color map where the red channel is assigned to orthopyroxene, green channel to olivine and blue channel to clinopyroxene. This lunar region appears as homogenous soil indicating the presence of high-Ca clinopyroxene. In contrast, the wall of Flamsteed P shows the presence of an admixed quantity of orthopyroxene and olivine.

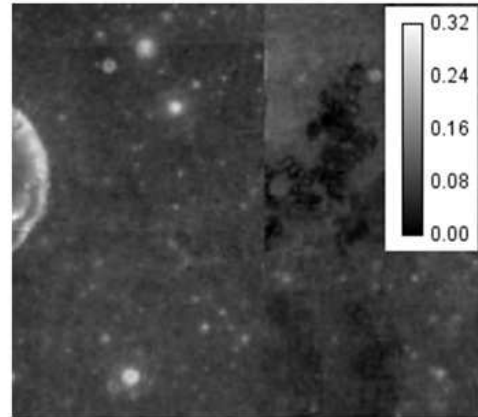
No significant differences are detectable in the maturation image of the examined region suggesting a high soil maturity.

To create a maturation image the 0.750/0.415 μm ratio image is assigned to the red channel, the 0.750/1.000 μm ratio image is assigned to the green channel and the 0.415/0.750 μm ratio image is assigned to the blue channel. In the maturation image immature surfaces appear greenish-blue while older mature soils appear reddish, the yellow color indicates freshly excavated basalt.

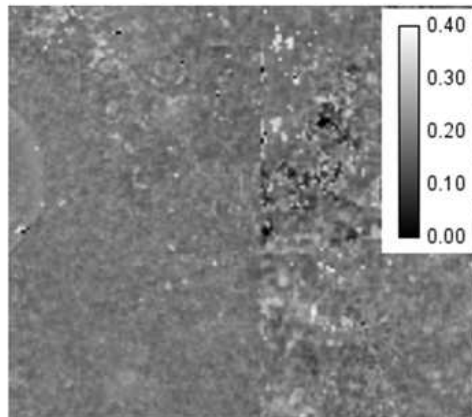
The process of surface maturation causes a reddening of the surface spectra (increase of a positive slope) and a decrease of the spectral contrast of the absorption bands.



Band center wavelength map



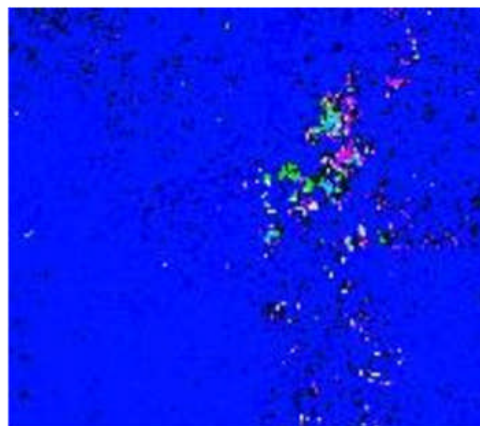
Band depth map



FWHM map

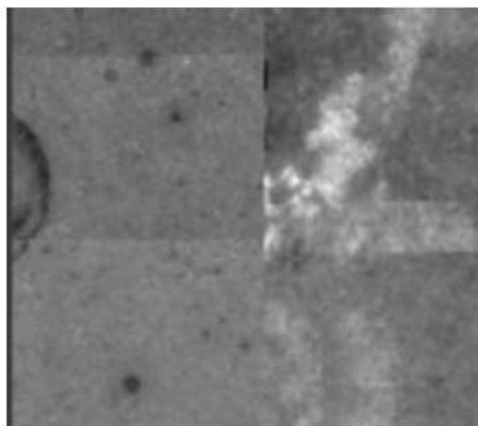


Maturation map



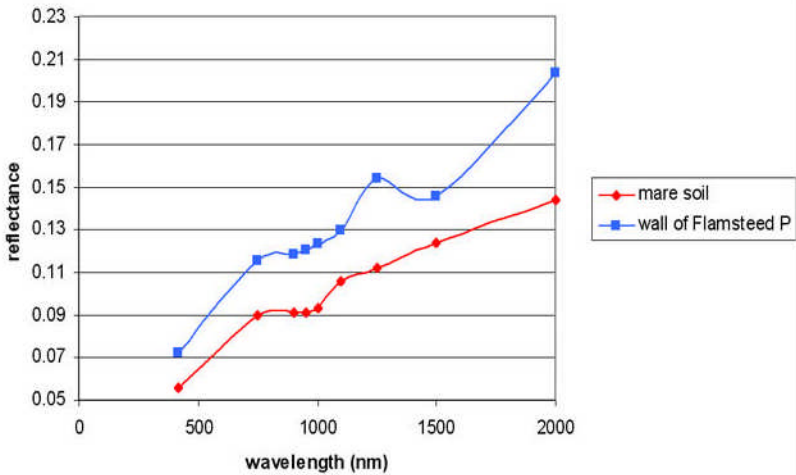
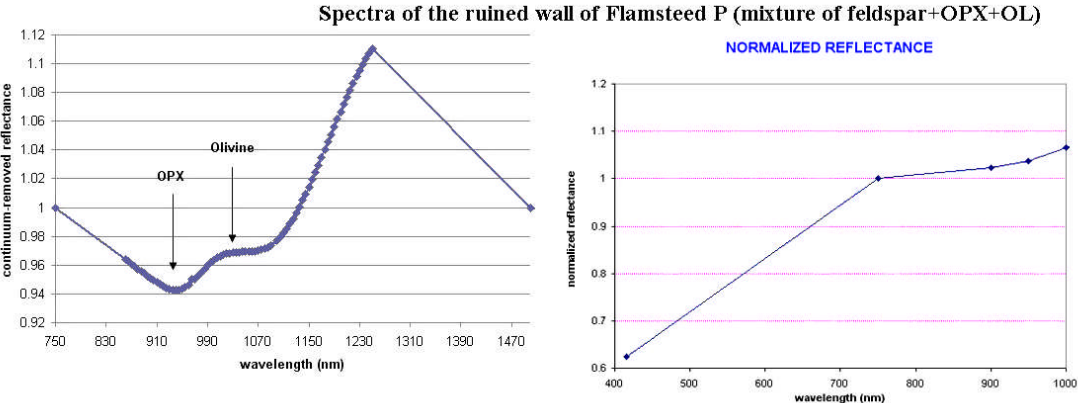
False color map

Red channel is assigned to orthopyroxene band center (0.890 to 0.945 μm), Green channel to olivine band centers (1.005 to 1.095 μm) and Blue channel to clinopyroxene band center (0.950 to 1.000 μm)



R_{2000}/R_{1500} ratio

The spectrum of the Flamsteed P wall shows an An2 signature using representative spectra for highland rocks (cf. section 6) taken by Tompkins and Pieters (1999). Moreover the continuum-removed reflectance spectrum shows a single absorption minimum and a broad olivine-related inflection feature. Plagioclase feldspar is spectrally characterized by a continuous upward slope from 415 to 900 nm and an absorption band at about 1300-1400 nm. Low-Ca pyroxene, which may be intermixed with plagioclase shows an absorption band at 940 nm. Hence, the spectral data indicate the presence of the plagioclase feldspar containing up mafic minerals composed of a mixture of orthopyroxene and olivine.



Working with very large Clementine UVVIS+NIR data files

Sometimes higher resolution studies of larger areas the size of the SPA basin or Mare Crisium require working with very large data files. A single band image in 16 bit tiff format might be as large as 7 Mb. Octave is too slow to analyze files sets of this size in a timely way and insufficient memory errors are also likely. When run for prolonged periods computers tend to develop secondary problematic issues with periodic automatic software updates, security checks, system hibernation etc. interfering with program completion and causing program "lock-ups." Images larger than 1500 x 1200 may cause issues. One way to avoid such problems and still work with large high resolution band image downloads is to slice the original band images into smaller subimage tiles in an automated fashion. We use the free program ImageMagick (an older version such as 6.5.7-Q16 is fine, but the version must be capable of working with 16 bit images). Use band images in 16 bit tif format.

Then, as an example for the 750 nm band image of size 3000 x 1600 pixels, at the command prompt for ImageMagick we use a command line such as:

```
> convert 750.tif -crop 600x400@ 750a.tif
```

The subimage block size here is selected is 600 x 400 pixels, but this can be varied as necessary. It is helpful for the original image to first be cropped to exact multiples of the desired width and height of the subimage block desired (this eliminates blocks of different sizes being created. When run on the original image described above, the result is a group of 20 sequential band subimages of size 600 x 400 pixels. The resulting image is opened using the File>Open command in ImageJ.

The resulting displayed image will have a slider at the bottom and it is possible to scroll through the 20 block images using it. Save the image as an image sequence in ImageJ using File>Save As>Image Sequence and choose txt format.

Maps can be made in Octave from each subimage and then the maps can be rejoined into a single high resolution map. This can be done in Photoshop manually, or a command at the ImageMagick prompt along the lines of that shown below can be used:

```
>montage -mode Concatenate -tile 5x4 750a_*.tif 750a_rejoined.tif
```

This will produce a single image from all subimage blocks. The specification `-tile 5 x 4` indicates that the subimage block set is to be assembled into a 5 x 4 matrix to reconstitute the original image dimensions. Image>Stacks>Make montage in ImageJ is an alternative for 32 bit tif or txt images. This option requires that the block images be imported as an image sequence (i.e. stack) in imageJ.

> 10. Production of Elemental Abundance Maps in Octave

Elemental abundance maps for Fe, Mg, Ca, Al, Ti, and O are easily produced from a data set of the three spectral parameter maps described above plus a map of the slope as given by the 0.75 micron Clementine band image subtracted from the 1.5 micron Clementine band image for the lunar feature of interest.

GLR has developed an automated Octave m file program, `applycoeff.m`, for this purpose. The Octave code is listed in Appendix 1. It requires input files within the same directory as `applycoeff.m` which are: `bandcenter.txt`, `banddepth.txt`, `fwhm.txt`, `750.txt` and `1500.txt`. The program automatically produces the slope map from the `750.txt` and `1500.txt` files. Other required files in the same directory are the matrix files: `matrix001`, `matrix003`, `matrix005`, `matrix007`, `matrix009` and `matrix0011`. These matrix files contain needed coefficients produced from a matrix regression of the spectral parameter maps and slope map on the lunar prospector elemental abundance map for each element for the global Moon. This has the

effect of greatly increasing the spatial resolution of lunar prospector elemental abundance data while producing a somewhat albedo resistant result. The theory for this is somewhat complicated and involves matrix algebra. It is beyond the scope of this manual, except to say that the matrix regression is based on $Ax=b$ where b is the lunar prospector elemental abundance map, x is the comparison matrix created from the band center, band depth, fwhm, and slope maps, and A is the coefficient matrix for the element of interest (given the name matrix001 etc. as described above).

Running `applycoeff.m` in Octave with the files described above present in the same directory, produces an output of 6 matrix files: `matrix002`, `matrix004`, `matrix006`, `matrix008`, `matrix010`, and `matrix012` which represent the elemental abundance maps for Fe, Mg, Ca, Ti, Al and O in that order.

These files are opened and saved using the same method as described above for the Octave produced maps `bandcenter`, `banddepth` and `fwhm`.

Required Coefficient Matrices

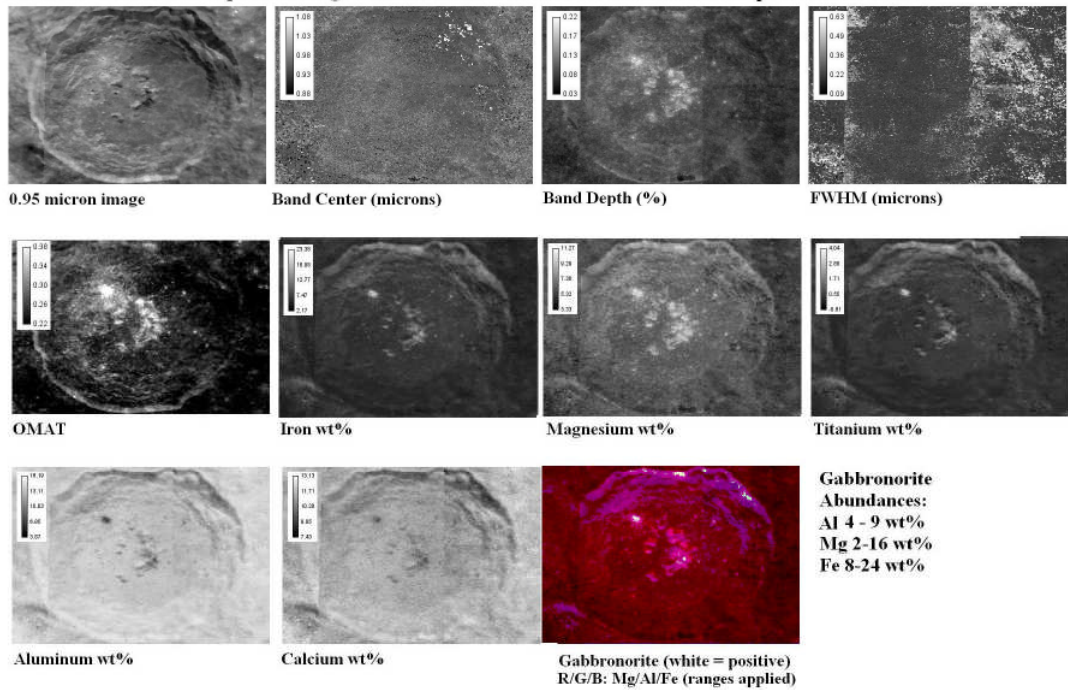
The required input coefficient matrices used by `applycoeff.m` are produced by another GLR Octave program, `newmatreg.m`, which creates them from input Clementine global lunar band images from 0.75 to 1.5 micron. The resulting matrix files: `matrix001`, `matrix003`, `matrix005`, `matrix007`, `matrix009` and `matrix011` represent the coefficients needed by `applycoeff.m` to calculate the elemental abundances for Fe, Mg, Ca, Ti, Al and O respectively.

These matrices can be made available to GLR members working in this area. This set of coefficient matrices is applicable to all lunar feature locations studied using `applycoeff.m`

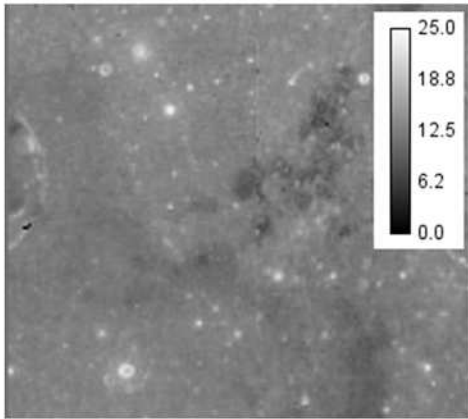
Example of Elemental Abundance Mapping

The elemental abundance maps for Stevinus below were produced using applycoeff.m

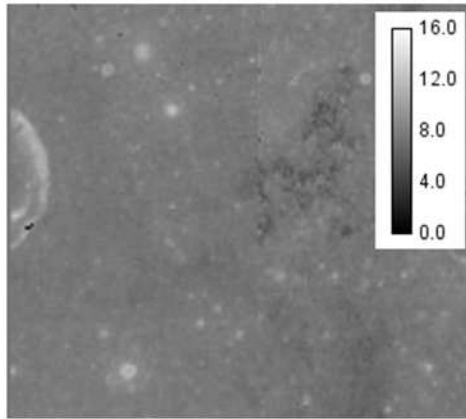
Stevinus Crater: Absorption Trough Parameter and Elemental Abundance Maps Made in Octave



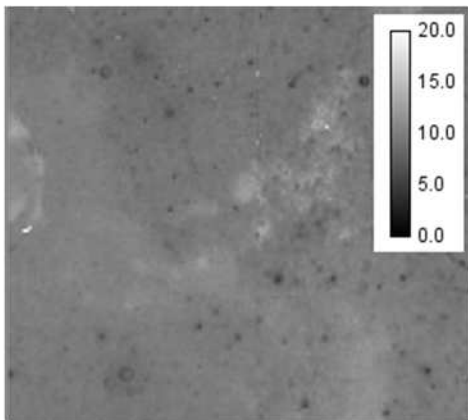
The elemental abundance maps for Flamsteed P region in the following figure were produced using applycoeff.m



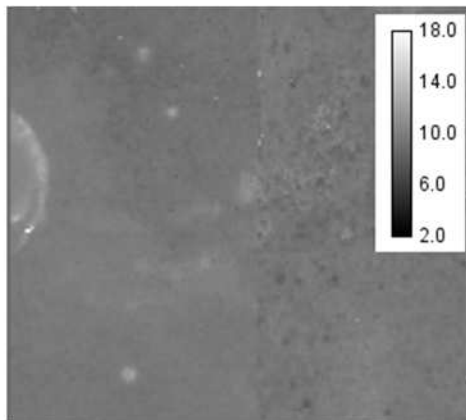
Fe wt%



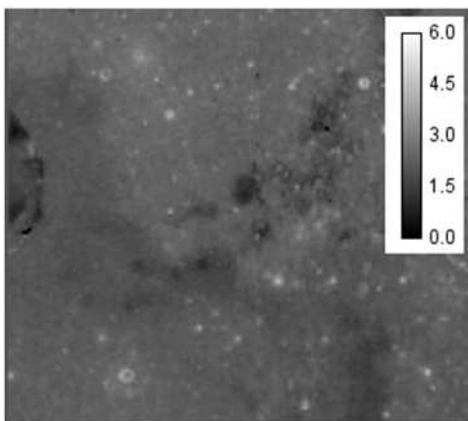
Mg wt%



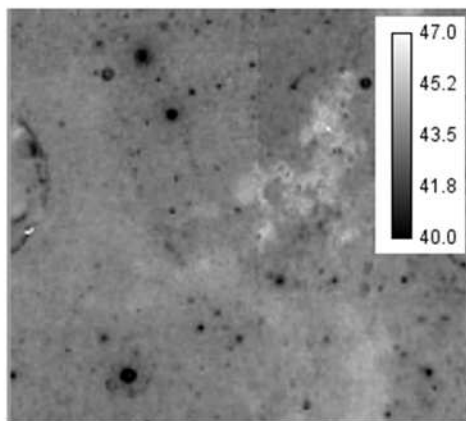
Al wt%



Ca wt%



Ti wt%



O wt%

Mineral Determinations

Note that the color map shown above for Stevinus crater is labelled gabbronorite. The gabbronorite composition is defined by certain aluminum, magnesium and iron elemental abundance ranges listed at the bottom right of the graphic. Using an analogous method, it is possible to produce mineral maps for FAN (ferroan anorthositic norite), norite, dunite, gabbronorite, troctolite, mare basalt, KREEP basalt, aluminous basalt, anorthosite, etc.

	Magnesium wt%	Aluminum wt%	Iron wt%
Ferroan anorthosite (FAN)	0 to 1.5	17 to 19	1 to 3
Troctolite	10 to 19	9 to 16	4 to 6
Mare basalt	4 to 8	4 to 7.5	12 to 25
Anorthositic norite	4 to 9	17 to 25	2 to 5
Norite	4 to 9	17 to 25	5 to 25
Gabbronorite	2 to 16	4 to 9	8 to 25
KREEP	2 to 4.5	8 to 10	8 to 9.5
Aluminous Basalt	4.2 to 7.2	>6.8	9.3 to 14.0

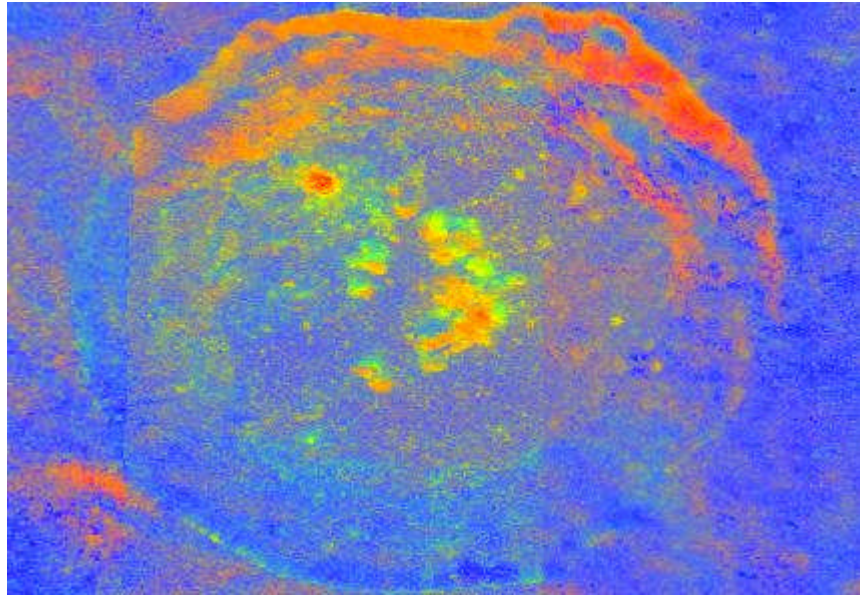
GLR has Octave m file programs to produce maps of each of these mineral types and can be made available to GLR members working in this area. The specific ranges are subject to vary according to the literature etc. These m files output maps of the pertinent elements but with range restrictions imposed (any other pixels being set to zero). These maps can then be placed in the RGB channels of a color image to create a false color map for the topographic location of the mineral under study. One such m program pair (read_from_ternary_diagram.m and applycoeff_v2.m) is based on three endmember (i.e. pure minerals) elemental abundances and is found at the end of Appendix 1.

These two m files function together to produce a petrographic map. The resulting petrographic map is saved as a 24-bit colour TIFF file named "petrographic_map.tif", in which the red, green, and blue channel represents the mare basalt, Mg-rich rock, and FAN endmember, respectively. The sum of the channels is always 255, as the endmember abundances always must sum up to 1. Both m files must be in the same directory as the input image files and matrix files.

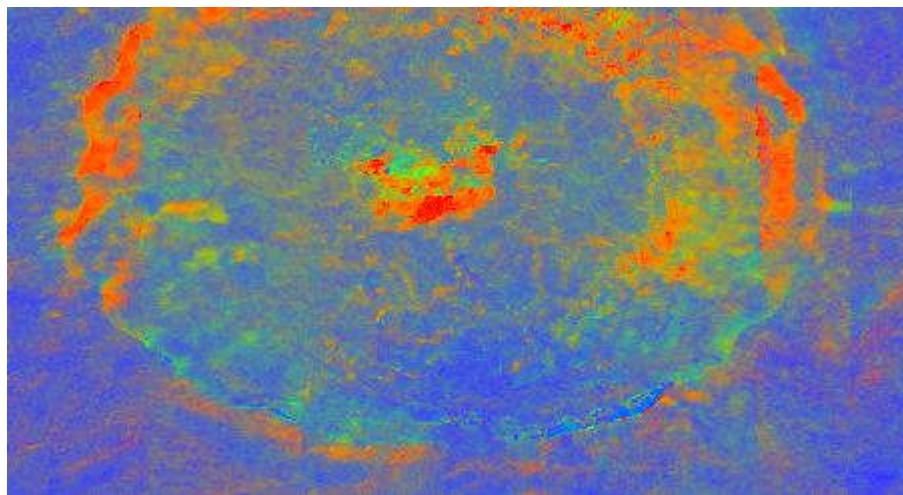
A petrographic map of Reine γ made according to the above description is presented below. For Reiner γ , we have mostly mare basalt, some Mg-rich rock, and nearly no FAN; that's why the petrographic map looks red-orange.



A petrographic map for Stevinus crater is shown below and here the presence of a greater concentration of magnesium rich rock, likely GNTA (i.e. gabbroic noritic troctolitic anorthosite) is shown in green and a fair amount of FAN (ferroan anorthosite) is shown in blue. Gabbroic rock relatively rich in clinopyroxenes is shown in red.

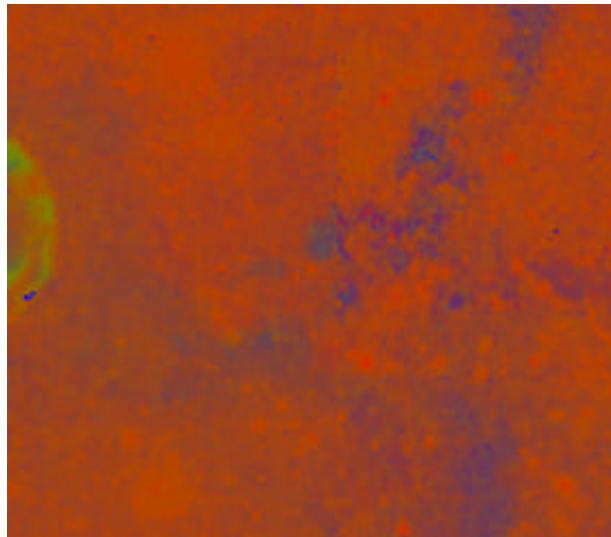


The petrographic map of Tycho below shows clinopyroxene containing gabbro to anorthositic gabbro in red, magnesium suite rock in green, and ferroan anorthositic rock in blue.

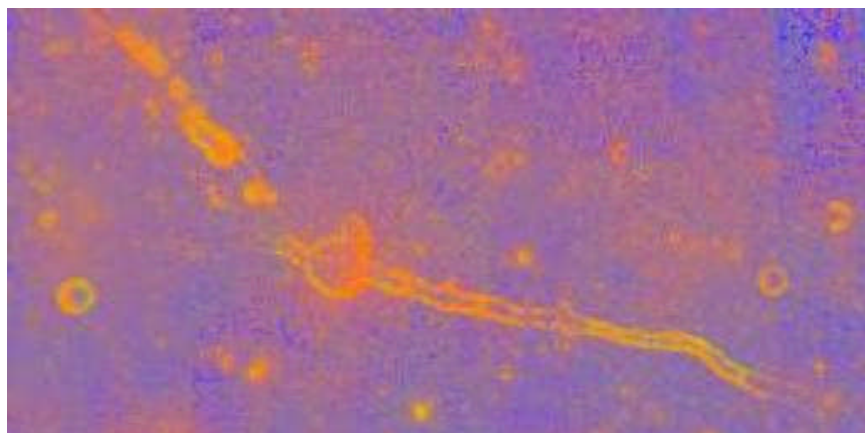


A petrographic map of Flamsteed P region made according to the above description is presented in the following figure. We determined the petrographic which indicates the relative fractions of the three endmembers mare basalt (red channel), Mg-rich rock (green channel), and ferroan anorthosite (FAN, blue channel). Accordingly we have

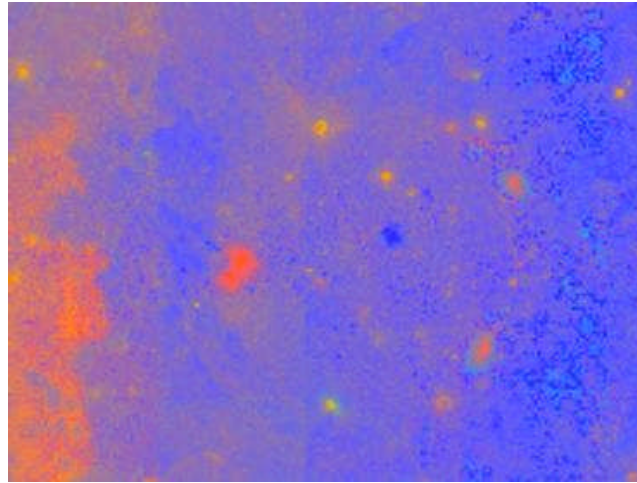
mostly mare basalt with some Mg-rich rock (the petrographic map looks orange). Furthermore the map shows the presence of magnesium suite rock (in green) in the wall of Flamsteed crater.



Petrographic maps of the Hyginus rille and of Alphonsus are shown below as further examples of the distribution of mare basalt, magnesium suite rock, and ferroan anorthosite. The map of the Hyginus rille shows mare basalt containing some olivine present along the rille structure. The adjacent terrain shows ferroan anorthosite mixed with mare basalt.



Hyginus Rille, petrographic map



Alphonsus, petrographic map

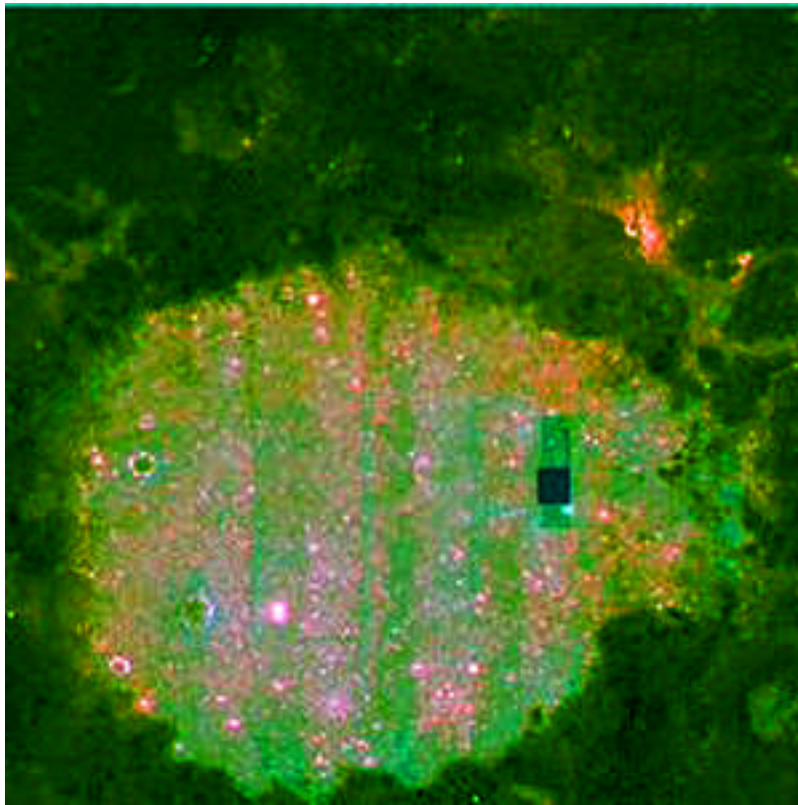
The petrographic map of Alphonsus shows basaltic material associated with the several volcanic vents present. The central peak is rather anorthositic as is much of the surrounding terrain until one reaches the basalt rich area to the west of the crater. Several small superficial craters may have penetrated down through the rather anorthositic surface into magnesian suite material.

Detection of Variations in Basalt Composition:

In addition to the standard petrographic maps described above, it is sometimes useful to map the distribution of basalts having slightly different compositions. Many different approaches can be taken, but one that is in current use by GLR is a basalt mapping in which average abundances of titanium and aluminum are used to differentiate different basalt types. For example, the following abundances can be assigned to the RGB channels of a false color image:

Red:	Ti 1.6 wt%	Al 9.25 wt%
Green:	Ti 0.5 wt%	Al 14 wt%
Blue:	Ti 3.6 wt%	Al 6.3 wt%

Typical mare basalts appear in the red channel, aluminous basalts and highlands type terrain appear in the green channel, and relatively higher titanium basalts appear in the blue channel. An application of this mapping technique to Mare Crisium is shown below. Highlands terrain has been masked.



The surface of mare Crisium and the southern portion of Mare Anguis have a basalt composition with a low titanium and high aluminum content. Reddish areas have higher titanium and lower aluminum content and represent older exposed subsurface basalts.

The Octave algorithm used to produce this mapping is `applycoeff_v3a` and its code is presented in the Appendix. Variations on this mapping theme can be tried using different elements and/or different wt % abundances by changing the parameters in this program code.

>11. Working with Selene Imagery

Calibration of Selene Multispectral Imager (MI) band images has currently reached level 2B2. This level of calibration basically includes radiometric calibration and conversion of output to radiance. In the future, 2C calibration will eventually become available and will include photometric calibration with conversion of output to reflectance and also a systematic geocorrection of image bands. However, even at the present stage of calibration, it is possible to use Selene data in a limited way to generate spectra of lunar features and to generate spectral maps. The purpose of Part I of this paper is to explain how to acquire Selene multispectral imager VIS and NIR band data and to further enhance its calibration for the purpose of generating relative reflectance spectra and producing maps of spectral features.

Part I: Selecting, Downloading, Converting and Saving Selene Archive IM Images

The Selene Multispectral Imager Dataset: General Description

The Selene (Kaguya) lunar probe acquired multispectral images at VIS and NIR wavelengths between September 2007 and June 2009. Five VIS bands were obtained at 0.415, 0.75, 0.9, 0.95, and 1.0 microns. Four NIR bands were obtained at 1.0, 1.05, 1.25, and 1.55 microns. The resolution of VIS bands is 20 meters/pixel. The resolution of NIR bands is 62 meters/pixel. These images have not yet been assembled into a fully calibrated mosaic as is the case for Clementine data, but they are available for download from the Selene Data Archive as single tile data. VIS five band images are packaged together in 16 bit unsigned data with Little Endian byte order with a variable length data header preceding the first image. There are no bytes between images

and the images are co-aligned. NIR four band images are packaged together in the same way. VIS and NIR images may or may not be offset from each other and it may well be necessary for the user to co-align VIS images with NIR images. VIS images are typically about 962 x 959 pixels although there is variation here. NIR images are typically about 320 x 319 pixels. Once the VIS images are re-scaled to the dimensions of NIR images, subpixel co-alignment (i.e. co-registration) may require more than applying a simple (x,y) pixel offset.

Finding a Lunar Feature in the Selene Archive and Downloading VIS and NIR data:

The first step here is to create an individual free account on the Selene Data Archive website at: <https://www.soac.selene.isas.jaxa.jp/archive/> which will enable access to the various Selene data products. Once logged into the data search system, it is necessary to specify the desired product. For the currently available Multispectral Imager data the product name is LISM 2B2. Pressing the “Determination” icon selects the listed product. Next, the time and date of the desired data is entered, but in practice it is enough to simply list the start date of September 14, 2007. The desired lunar feature is selected using the Observation Range menu, by simply pressing the Setup Observation Range icon. This will lead to the generation of a lunar map. The user simply draws a box around the target area of interest and zooms the image. A fairly high zoom level is usually desirable. Individual Selene VIS and NIR data tiles are not much larger than the area covered by Copernicus Peak 3. The icon labelled “Determination of Selection Range” is pressed to send the longitude and latitude coordinates of the area of interest to the main search page. All necessary constraints have now been chosen and the “Search Execution” icon can be pressed to access the available band data.

Available data tiles will be listed but it will be necessary to select VIS or NIR image groups separately. Thumbnails of the feature can be

viewed to aid in the selection of VIS and NIR image packages. Care should be taken to choose VIS and NIR image packages that show exactly or at least nearly the same geography (some offset may be present between the image groups). Desired packages are added to an order list which is then confirmed by the user. NIR and VIS files are chosen separately. The Selene archive will send a confirmation of the order and in a second email will specify a download address.

Working with Downloaded Selene Archive VIS and NIR Data Packages

Downloaded VIS and NIR packages will be in .sl2 format. Windows users should convert the file extension to a .tar extension. This will allow unzipping each package using common programs such as WinZip. Several files are present within each package, but the important file is actually a zipped file with the extension .igz. It is necessary to change this extension to a .gz extension which then allows it to be opened with WinZip, gzip etc. When this file is unzipped, the most important resulting file has an .img extension. This file contains the archived image bands and a preceding header with lots of image data. The file is in an unusual .pds type image format which most programs cannot read. We generally make a copy of the .img file and give it the extension .pds for reasons that are explained below.

Using ImageJ to Open the .img file

ImageJ is a free image processing program. It is available for download at: <http://rsbweb.nih.gov/ij/download.html> but to use it to work with Selene .img files it is necessary to download an additional free plugin called the Raw File Opener which is found under the Input/Output section here: <http://rsbweb.nih.gov/ij/plugins/index.html>

Simple instructions for installing the plugin are present on at the download site: <http://rsbweb.nih.gov/ij/plugins/raw-file-opener.html>

When it is installed and working, the Raw File Opener is selected from within the ImageJ menu: Plugins > Input-Output > Raw File Opener.

Reading Image Header Information

Using File > Open in ImageJ, the copy of the .img file that was renamed to a .pds extension can be viewed, but only the header information will be legible. However, reading the header information will give some key pieces of information needed to unpack the images in the VIS and NIR .img files. Files will always be in 16 bit unsigned format with Little Endian byte order and zero bytes between images. VIS .img files will contain five image bands and NIR .img files will contain four image bands. But header information will give the image width and height and the number of header bytes present before the first image. These should all be recorded.

Opening the .img image package for VIS and NIR

VIS and NIR .img files are opened in ImageJ using the Raw File Opener plugin: Plugins > Input-Output > Raw File Opener. Information present in the header information must be entered and is different for VIS and NIR .img files. Image dimensions can vary slightly for different geographical areas imaged as well. For the most part, NIR files are about 320 x 319 pixels and VIS files are roughly 962 x 959 pixels.

When an image is opened successfully it will open in an image sequence viewing box with four bands for NIR and five bands for VIS which can be viewed by moving a slider at the bottom of the image sequence viewing box in ImageJ. Each image should have the appearance of the thumbnail image included in .jpg format in each download. If the images are distorted or skewed then most likely small variations will be needed to adjust the image dimensions. Sometimes very small adjustments to the dimensions given in the header are

needed.

Each image should be saved as a 32 bit tiff image Image > Type >32 bit and the VIS images should be re-scaled to the dimensions of the NIR images. When this is done, the VIS+NIR images can be opened as a single image sequence in ImageJ (see below). The nine VIS+NIR image bands should be saved to their own directory. The name of each tif image should be changed to its band wavelength keeping the tif extension. Use 1000.tif for the VIS 1000 nm band and 1000a.tif for the NIR 1000 nm band image. When Import > Image Sequence is selected in ImageJ, clicking on the first band image will allow the entire group to be imported.

Saving the VIS and NIR images in 32 bit tif format

When the VIS and NIR images are opened, they are best changed to 32 bit tiff type if this was not done previously. This is achieved as follows: Image > Type >32 bit and their image groups are saved as separate image sequences as follows: File > Save As > ImageSequence > tif.

Each individual image within the VIS and NIR groups are thereby saved as individual tif images in 32 bit format. If necessary, the brightness and contrast of the images can be altered without changing the pixel values as follows: Image > Adjust > Brightness and Contrast. The images should be re-named according to their band wavelength and saved in 32 bit tiff format. It is convenient to name the 1000 nm VIS image as 1000.tif and the 1000 nm NIR image as 1000a.tif.

Co-Alignment of VIS+NIR band images

If when viewing the image sequence of all VIS+NIR band images, it is obvious that the two groups of images are offset from each other, then it will be necessary to co-align them to subpixel accuracy. This must be done using software capable of working with 32 bit images. We generally open the NIR and VIS bands as two separate image groups in

ImageJ and place them side by side. We crop each set to make them as identical topographically as possible and resize the VIS image sequence to the same dimensions as the NIR image sequence. Any ragged edge artifacts need to be cropped out. After this is done, the VIS+NIR image stack is then image stabilized using the image stabilizer plugin for ImageJ. If alignment still isn't good (which is rare), sometimes use the commercial program MiraPro 7 to do a multipoint alignment and then repeat the image stabilization. Instructions for the co-alignment process using this software package are beyond the scope of this paper, but are included in the manual for MiraPro 7.

Part II: Generating Spectra and Spectral Maps using Selene IM images

Image Re-Calibration

Method 1: Using Apollo 16 site and Apollo 16 Soil Sample 62231

The VIS + NIR band images as a 9 image group are loaded into ImageJ as an ImageSequence. This is facilitated by putting only these 9 images into their own directory and when opening the Image Sequence, only the first tif file is selected. All of the images will automatically be opened in the image sequence in order of increasing band wavelength.

There are two different approaches to image calibration each with its good and bad points. One method is to select the Apollo 16 landing site as the first set of VIS and NIR images downloaded from the Selene Archive.

The VIS + NIR band images as a 9 image group are loaded into ImageJ as an ImageSequence. This is facilitated by putting only these 9 images

into their own directory and when opening the Image Sequence, only the first tif file is selected. All of the images will automatically be opened in the image sequence in order of increasing band wavelength.

Step 1: Image Normalization for Apollo 16 Site Band Images

With the Image Sequence opened, an area of medium albedo within the Apollo 16 site is selected using the “box” icon on the ImageJ menu. It should be on the order of 1000 or so pixels in size. As the slider is moved at the bottom of the viewer, the next band image will appear, but the boxed area remains in the same position. Pressing Control-H will bring up the histogram data window and the average pixel DN value can be read. It should be recorded for each of the nine band images. The box is then removed by clicking anywhere on the selected image.

Each band image is mathematically divided by the recorded histogram average pixel DN value recorded for the boxed area as described above. This is done in ImageJ by:

Process > Math > Divide. When the division is made ImageJ asks if the division is to be applied to the currently selected image or to all images. It should be applied only to the currently selected image. The next image is then selected and divided by its boxed histogram value, and the next, and so on until all nine images have been “normalized”.

If after the normalization process is completed, all of the band images do not have quite nearly the same DN value for a selected large pixel block area, then most likely the Apollo 16 site is not a good calibration site for the data set under study. When this is the case, it is usually the 0.415 or the 0.749 micron bands that will appear brighter than the other bands after normalization, indicating a bad calibration result is likely to occur. When this happens, we usually abandon Method 1 and try to move on to Method 2. However, if the the problem is only with the

0.415 micron band then this band is not essential to determination of the trough parameters close to 1 micron and Method 1 can still be used for this work. It is essential, however, that the 0.749 micron band be well normalized.

Step 2: Image Re-Calibration for Apollo 16 Band Site Images

The file RELABBDR.TAB is downloaded from the PDS Geosciences Node found here:

<http://pds-geosciences.wustl.edu/missions/lunarspec/>

This file is opened in Excel or a similar spreadsheet program. The file contains calibration correction gain coefficients based on Apollo 16 soil sample #62231 converted to bidirectional reflectance (bidirectional reflectance is used to correct lunar probe data while hemispheric reflectance is used to correct Earth based telescope data).

The calibration factor for each Selene VIS and NIR band should be recorded from the relabldr.tab file. Interpolation is necessary for many of the bands. Using ImageJ, each previously normalized Apollo 16 Selene band image is multiplied by its corresponding correction factor. The image sequence is then saved as a series of 32 bit tif images. Feel free to adjust the brightness and contrast of 32 bit tiff images as this does not affect their pixel values.

The Selene VIS and NIR band images of the Apollo 16 site has now been completed and can be used for calibration of Selene data for other lunar features. The calibrated Apollo 16 site images should be viewed as an image sequence in Image J and the average DN balue of the Apollo 16 site determined for each band image using the histogram function. The values should be recorded for each band.

Step 3: Calibration of other lunar features against the Selene Apollo 16 site.

Normalization:

A second set of Selene images is downloaded for the lunar feature of interest. The target images are normalized by dividing each band image by the histogram value of the un-normalized and uncalibrated (except for the 2B2 pre-calibration already present in downloaded Selene imaging spectrometer images) Apollo 16 site image of the same band wavelength. This is done in ImageJ as described above.

Calibration:

The normalized VIS+NIR band images of the lunar feature of interest are then calibrated by multiplying each band image by its corresponding correction coefficient found in the relabldr.tab file previously discussed.

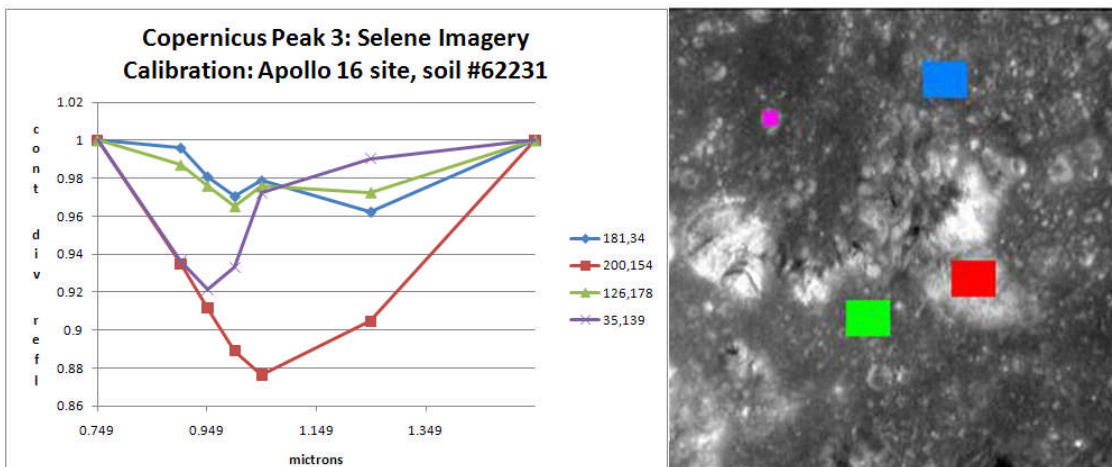
This completes the calibration of the VIS+NIR band images of the target feature of interest against the Apollo 16 site and Apollo 16 soil sample 62231.

Because the Selene 2B2 calibration does not involve geocorrection, however, it is possible that re-calibrated images using this method might have some residual error.

Therefore Method 2 outlined below is provided for comparison purposes. Method 2 is based on Mauna Kea 2.2 meter telescope 120 color spectra calibration and has the advantage of more nearly eliminating the distance between the calibration site and the target site under investigation. Calibration data obtained with the Mauna Kea 2.2 meter telescope and McCord circular variable filter (CVF) NIR Photometer is available from the PDS Geosciences Node as described below.

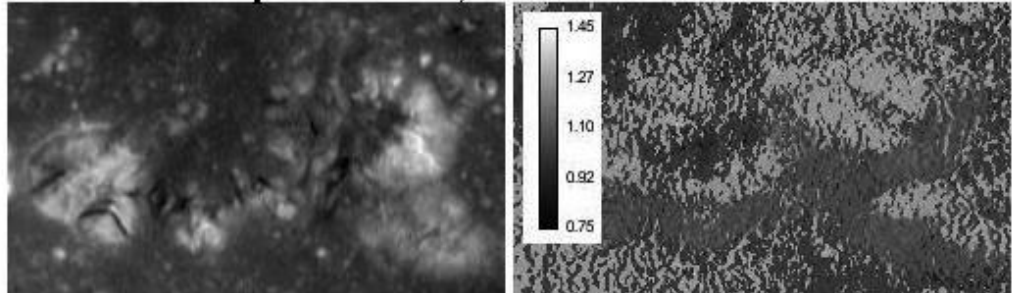
The results of this calibration are shown in the two figures below. Block spectra were measured using ImageJ v 1.43J and spectral maps were made in Octave.

Block Spectra, Copernicus Peak 3, Apollo 16 and soil #62231 calibration



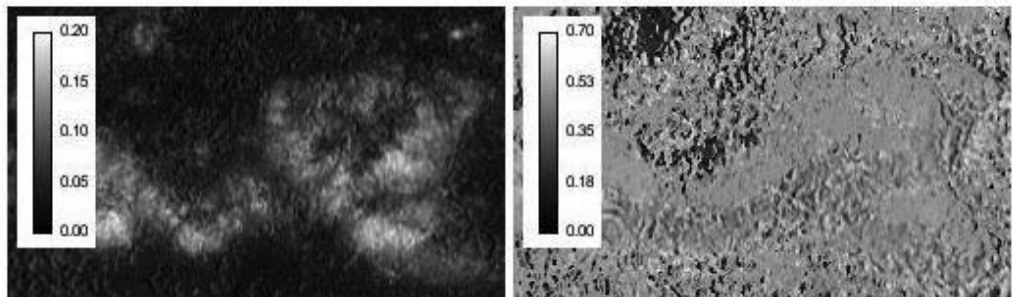
Spectral Maps, Copernicus Peak 3, Apollo 16 and soil #62231 calibration

**Copernicus Peak 3: Selene Imagery.
Calibration: Apollo 16 site, soil #62231.**



0.95 micron image

Band center map (microns)



Band depth map (%)

FWHM map (microns)

Maps made in Octave

Method 2: Using Mauna Kea 2.2 meter telescope 120 color spectra for calibration

Mauna Kea 2.2 meter telescope 120 color spectra are available for a large number of lunar features and have been pre-calibrated to the Apollo 16 soil sample 62231. Since they are in hemispheric reflectance, each band must be multiplied by a bidirectional reflectance correction coefficient. Both the Mauna Kea 2.2 meter telescope 120 color spectra and the bidirectional reflectance correction file can be downloaded from:

<http://pds-geosciences.wustl.edu/missions/lunarspec/>

The name of the bidirectional reflectance correction file is: CORRBDR.TAB

By referring to the index which is included in the Mauna Kea 2.2 meter 120 color spectra download, one of the Mauna Kea 2.2 meter telescope spectral data files closest to the target feature of interest is chosen and reflectance values are multiplied by the bidirectional reflectance constant for each of the Selene VIS+NIR wavelengths of the target feature VIS and NIR datasets that were downloaded from the Selene Archive.

The target feature VIS+NIR spectra are normalized by selecting the same boxed pixel area for each of the band images and obtaining an average DN value for the boxed area using the histogram function in ImageJ as was described above. The boxed area should be near, but not identical to the longitude and latitude of the Mauna Kea 2.2 meter telescope calibration file to be used. Each VIS+NIR band is then divided by its histogram box average DN value. This serves to normalize the nine image bands. This is done as previously described, using the math function in ImageJ within an imported image sequence of the nine spectral band images in 32 bit tiff format.

Normalization Area for Copernicus Peak 3 is boxed

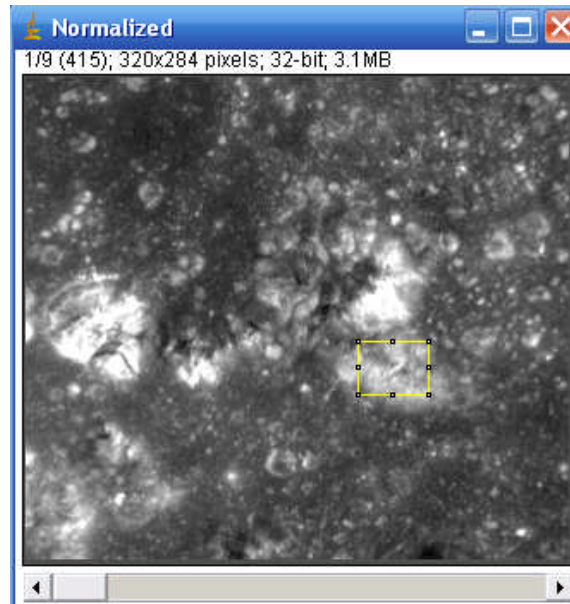


Finally, the normalized bands are multiplied by the bidirectional reflectance corrected Mauna Kea 2.2 meter telescope spectral values for the adjacent calibration site. Mauna Kea 2.2 meter telescope data begins at about 0.62 microns, so it is not possible to calibrate the 0.415 micron Selene VIS image band. This is not very important since only the 0.75 to 1.55 nm bands are useful in evaluating the absorption trough near 1000 nm which is essential to mineral identification.

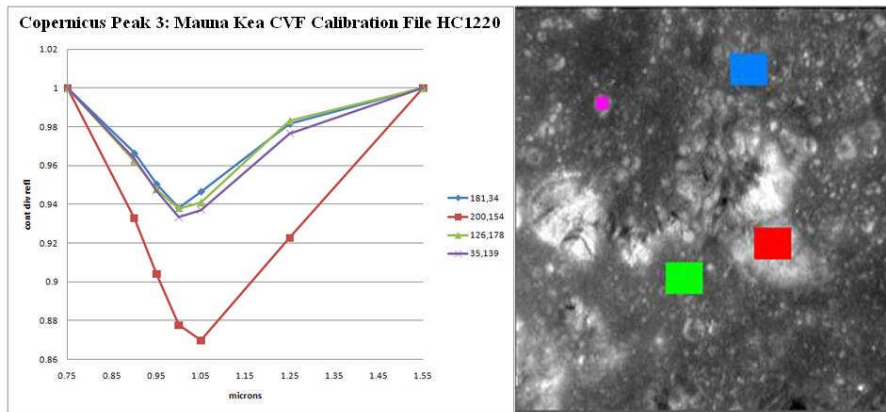
The disadvantage of Method 2 is that it sacrifices the 0.415 band calibration but its advantage is that the calibration and target sites will be much closer to each other than the target site would be to the Apollo 16 site used in Method 1.

Results of the calibration using Method 2 are shown in the block spectra and spectral map figures below.

Copernicus Peak 3 target area (181,34) boxed

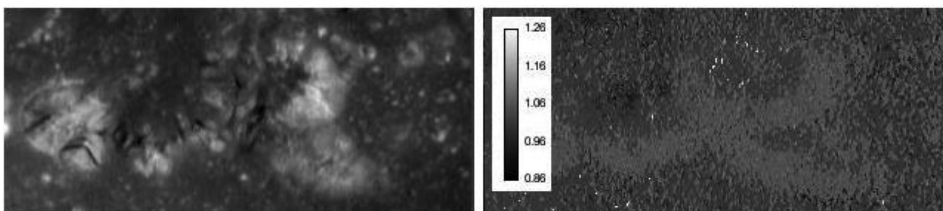


Copernicus Peak 3, Mauna Kea CVF file HC1220 calibration



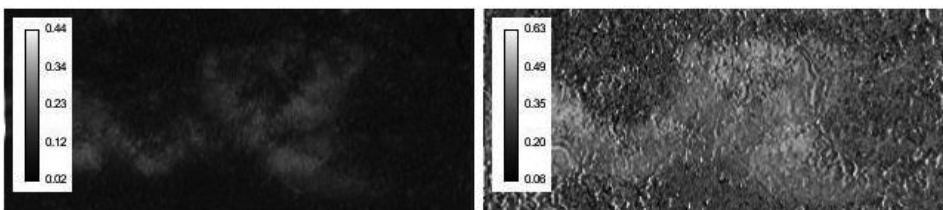
Copernicus Peak 3, Mauna Kea CVF HC1220 calibration. Spectral Maps

Copernicus Peak 3: Selene Imagery Calibration: Mauna Kea CVF file HC1220



0.95 micron image

Band center image (microns)

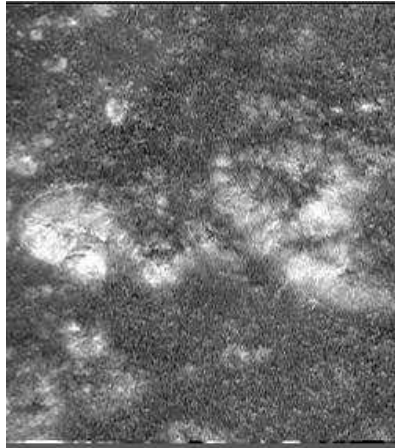


Band depth image (%)

FWHM (microns)

Maps made in Octave.

OMAT map (optical maturity map) Bright: 0.3, Dark: 0.1
Prepared from Mauna Kea CVF calibration.



Other Calibration Methods

For geographic areas where the Clementine UVVIS+NIR data do not show the effects of thermal sensor instability in the NIR, it is possible to use the Clementine imagery to calibrate Selene imagery of the same general terrain. This is done procedurally much like the Mauna Kea 2.2 m telescope with CVF example above, except that the Mauna Kea calibration file would be replaced by calibrated Clementine UVVIS+NIR spectra normalized to the 0.75 micron image. After normalizing the selene imagery using a selected pixel block corresponding to the Clementine geography, the calibrated Clementine spectral data for each band would be used as a multiplier for the corresponding Selene band. It is, naturally necessary to interpolate some values such as the 1.049 micron and 1.548 micron values and a simple spline interpolation is useful for this purpose. We achieved a successful calibration of gamma Reiner using this method which was chosen because the Apollo 16 site did not normalize the Selene 0.749 band well and a Mauna Kea 2.2 m CVF data file was not available for the general area of gamma Reiner.

Results:

Evaluation of Mineral Content via characteristics of the iron absorption trough near 1 micron have been discussed in detail in prior Selenology Today articles including:

Evans, R. Analysis of Lunar Spectra and Multiband Images (2007) Selenology Today Vol. 7. pp. 1-46.

which can be downloaded here: <http://digilander.libero.it/glrgroup/journal.htm>

To summarize, calibrated Selene spectral band DN values obtained using Method 1 or Method 2 above, for a boxed pixel area centered on the target site of interest are obtained from 0.75 to 1.55 microns using the described techniques in ImageJ. The DN values of all bands are divided by the DN value of the 0.75 micron band, which serves to normalize the spectra. The normalized spectra are plotted on a relative reflectance vs wavelength plot and a line through (0.75, 1) and (1.55, y) is taken tangent to the spectral curve, where y is the relative reflectance of the normalized 1.55 micron band for the target feature. Next the spectral curve is divided by the tangent line. This is achieved for each wavelength band by dividing the relative normalized reflectance for that band by

[(the band wavelength in microns * slope of the tangent line) + y-intercept of the tangent line)].

The plot of the resulting curve vs the band wavelength is the continuum divided spectrum and is extremely useful in evaluating the iron absorption trough near 1 micron. This plot has the characteristic that the relative reflectance of the 0.75 micron and the 1.55 micron band will be 1.0. The band center of a trough between these wavelengths and

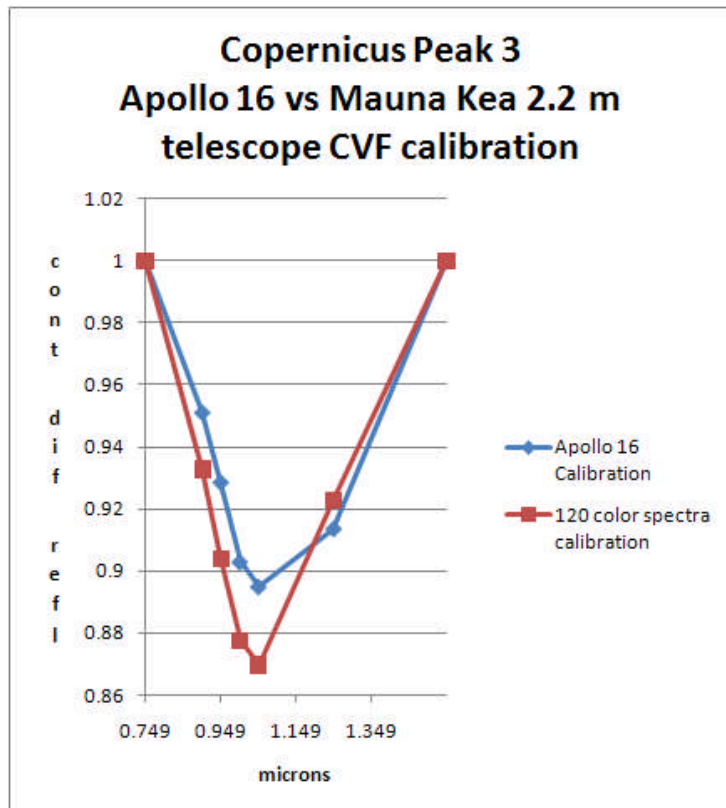
the percent depth of the trough are significant in assessment of mineral content as explained in the referenced paper in more detail.

Creation and interpretation of Spectral maps using VIS+NIR spectra is explained in:

Evans R, Woehler C, and Lena R: Spectral mapping using Clementine UV-Visible-NIR Data Sets: Applications to Lunar Geologic Studies. (2009) Selenology Today, Vol. 14 pp. 1-70.

which can be downloaded here: <http://digilander.libero.it/glrgroup/journal.htm>

Comparison of Mauna Kea 2.2 meter telescope based and Apollo 16 site based calibrations



Selene VIS+NIR spectra calibrated using Mauna Kea 2.2 meter telescope 120 color spectra corrected to bidirectional reflectance gave good results when applied to central peak 3 of Copernicus. The continuum divided spectra of the absorption trough near 1 micron appear to be less noisy than prior results I have obtained using Clementine UVVIS+NIR spectra with the standard Clementine USGS calibration based on the Apollo 16 site and Apollo 16 soil sample 62231. Results for peak 3 of Copernicus in this study are consistent with a significant olivine composition.

Amateur astronomers interested in lunar geology can use this method to obtain spectra and spectral maps of geologic lunar features of interest using the present 2B2 calibration of Selene multispectral imager band images. Two methods by which this 2B2 calibrated data set can be re-calibrated for evaluating the key iron absorption trough near 1 micron are discussed. They each have advantages and disadvantages. Use of Method 1 based on the Apollo 16 site and Apollo 16 soil sample 62231 has the disadvantage that target areas of interest will likely be geographically from the calibration site, but calibration of the 0.415 micron band is achieved. Use of Method 2 based on Mauna Kea 2.2 meter telescope 120 color spectral data pre-calibrated to the Apollo 16 soil sample 62231 has the advantage that its large number of geographic calibration sites means that a target area of interest is likely to be relatively close to a calibration site, at least as compared to a calibration using the Apollo 16 site such as Method 1. However, Mauna Kea 2.2 meter telescope 120 color spectra data cannot be used to obtain a calibration of the 0.415 micron band image.

This paper is limited to block spectra and spectral mapping of Copernicus central peak 3 based on either Apollo 16 and soil # 62231 or Mauna Kea 2.2 meter telescope 120 color spectrum calibration of the

Selene 2B2 VIS+NIR band images. Comparison of the block spectra and maps derived for these two calibration methods are present for comparison purposes. For the most part the block spectra are quite similar, although some variation is present for the site with pixel coordinates of approximately (35,139), i.e. the purple block spectra curve, which may reflect sampling error for this particular site. Comparison of the spectral maps also shows that they are quite similar.

> 12. Conclusion

This manual is intended as an introductory guide to GLR activity in lunar mineral studies and will evolve with time. Hopefully it will serve as the basis of ongoing discussion and learning for GLR members.

>13. Suggested Reading List

Arthur, D.W.G., (1962).Some systematic visual lunar observations.Comm.LunarPlanet.Lab.4,317–324.

Chevrel, S.D., Pinet P.C., et al. (2004) Composition and Structural Study of the Aristarchus Plateau from Integrated UV-VIS-NIR Spectral Data. Lunar and Planetary Science XXXV.

Evans, R., Wöhler, C., and Lena, R., (2009). Spectral mapping using Clementine UV-Visible-NIR Data Sets: Applications to Lunar Geologic Studies. Selenology Today, Vol. 14 pp. 1-70.

Evans, R, Wöhler, C., (2010). Archimedes: A spectral study of the south rim "red spot" anomaly. Selenology Today Issue , Vol. 17 pp.53-77.

Evans, R., (2007). Analysis of Lunar Spectra and Multiband Images. *Selenology Today* Vol. 7. pp. 1-46.

Evans, R. (2007) Calibration of small telescope lunar spectral images using Mauna Kea 2.2 meter telescope 120 color reflectance data. *Selenology Today*, Vol 10 pp. 26-33.

Fielder, G., (1965). *Lunar Geology*. Lutterworth Press, London.

Flor, E.L., Jolliff, B.L., Gillis, J.J., (2003). Mapping the concentration of iron, titanium, and thorium in lunar basalts in the western Procellarum region of the moon. *Lunar and Planetary Science XXXIV*, abstract#2086.

Gaddis, L.R., Staid, M.I., Tyburczy, J.A., Hawke, B.R., Petro, N.E., (2003). Compositional analyses of lunar pyroclastic deposits. *Icarus* 161, 262–280.

Giguere, T., Taylor, G.J., Hawke, B.R., Lucey, P.G., (2000). The titanium contents of lunar mare basalts. *Meteoritics and Planetary Science*. Vol 35. 193-200.

Gillis, J.J., Jolliff, B.L., Korotev, R.L., (2004). Lunar surface geochemistry: global concentration of Th, K and FeO as derived from lunar prospector and Clementine data. *Geochimica and Cosmochimica Acta*. Vol 68(8) pp. 3791-3805.

Head, J.W., III, Wilson, L., (1979). Alphonsus-type dark-halo craters: morphology, morphometry, and eruption conditions, in: *Proc. Lunar Planet. Sci. Conf. 10th*, pp. 2861–2897.

Le Mouelic, S., Langevin, Y., Erard, S., (1999). Discrimination between Olivine and Pyroxene from Clementine NIR data: Application to Aristarchus Crater. LPSC XXX

Lucey P.G., Blewett, D.T., and Hawke, B.R (1998). Mapping the FeO and TiO₂ content of the lunar surface with multispectral imagery. J. Geophysical Research Vol. 103 No. E2 pages 3679-3699.

Lucey. P.G., Taylor, J.G., and Hawke, B.R., (1998). Global Imaging of Maturity: Results from Clementine and Lunar Sample Studies. Lunar and Planetary Science X X I X .

Ohtake, M., Demura, H., Haruyama, J., Hirata, N., Nakamura, R., Sugihara, T., Takeda, H. (2003). Study of the Optical Standard Site for the Selene Multiband Imager. Lunar and Planetary Science XXXIV abstract 1976.

Ohtake, M., Haruyama, J., Mastunaga, T., Yokota, Y., Morota, T., Honda, C., Torii, M., Ogawa, Y. First Results of the Selene Multiband Imager. Lunar and Planetary Science XXXIX abstract #1568.

Ohtake, M., Arai, T., Takeda, H., (2005). Study of the Apollo 16 Landing Site as a standard site for the Selene Multiband Imager. Lunar and Planetary Science XXXVI abstract #1637.

Pieters, C.M. and Englert, P.A.J. Topics in Remote Sensing 4: Remote Geochemical Analysis: Elemental and Mineralogical Composition. Chapter 14: Compositional Diversity and Stratigraphy of the Lunar Crust Derived from Reflectance Spectroscopy. pp. 309-342. Cambridge University Press 1993 (ISBN: 0-521-40281-6).

Tompkins, S., and Pieters, C.M., (1997). Composition of the Lunar Crust Beneath the Megaregolith, LPSC XXVIII, LPI, Houston, TX 1439-1440.

Tompkins, S. (1998). Mafic Plutons in the Lunar Highland Crust. LPSC XXIX

Tompkins, S., Margot, J.L., Pieters, C.M., (2000). Effects of topography on interpreting the composition of materials within the crater Tycho. Lunar and Planetary Science XXXI, abstract #1401.

Weitz, C.M., Head, J.W., (1999). Spectral properties of the Marius Hills volcanic complex and implications for the formation of lunar domes and cones. J. Geophys. Res. 104 (E8), 18933–18956.

C. Wöhler, A. Berezhnoy, R. Evans, (2009). Estimation of Lunar Elemental Abundances Using Clementine UVVIS+NIR Data. European Planetary Science Congress. EPSC 2009-263

Appendix 1: Octave Code

Program Code for ClementineMaps.m:

```
% Algorithm to Extract bcw, depth and fwhm from Clementine 750 nm thru
1500 nm imagery

% load Clementine txt images from c:\Octave\ClemArchimedes 750nm to
1500 nm and assign % to A1 thru A7

A1 = dlmread ("750.txt");
A2 = dlmread ("900.txt");
A3 = dlmread ("950.txt");
A4 = dlmread ("1000.txt");
A5 = dlmread ("1100.txt");
A6 = dlmread ("1250.txt");
A7 = dlmread ("1500.txt");

% Create a 7 dimensional matrix D whose sheets are A1 through A7

D(:, :, 1) = A1;
D(:, :, 2) = A2;
D(:, :, 3) = A3;
D(:, :, 4) = A4;
D(:, :, 5) = A5;
D(:, :, 6) = A6;
D(:, :, 7) = A7;

% Create a 7 dimensional matrix E whose sheets are all A1

E(:, :, 1) = A1;
```

```
E(:, :, 2) = A1;
E(:, :, 3) = A1;
E(:, :, 4) = A1;
E(:, :, 5) = A1;
E(:, :, 6) = A1;
E(:, :, 7) = A1;

[nr,nc] = size(A1);

% Normalize all Selene image bands to 750 nm band image
N = D./E;

%Start of Main Algorithm

r = 0;
c = 1;
% *****

for d = 1:nr*nc;

r = r + 1;

if r == nr + 1;
    r = 1;
    c = c + 1;
endif
```

```

if c == nc + 1;
    c = 1;
endif

% Calculate Continuum line for first pixel

slope = (N(r,c,7) - 1)/0.750;
intercept = -1 * ((slope * .750) -1);

% Continuum divided spectra

x1 = 0.750*slope + intercept;
x2 = 0.900*slope + intercept;
x3 = 0.950*slope + intercept;
x4 = 1.0*slope + intercept;
x5 = 1.1*slope + intercept;
x6 = 1.25*slope + intercept;
x7 = 1.5*slope + intercept;

M(r,c,1) = N(r,c,1)/x1;
M(r,c,2) = N(r,c,2)/x2;
M(r,c,3) = N(r,c,3)/x3;
M(r,c,4) = N(r,c,4)/x4;
M(r,c,5) = N(r,c,5)/x5;
M(r,c,6) = N(r,c,6)/x6;
M(r,c,7) = N(r,c,7)/x7;

```

```
% apply cubic spline for continuum divided spectral data

H = [.750 .90 .950 1.0 1.1 1.25 1.5];
I = [M(r,c,1) M(r,c,2) M(r,c,3) M(r,c,4) M(r,c,5) M(r,c,6) M(r,c,7)];

% interpolate spline using Akima Interpolation at approx. 1 nm
intervals

xi = [linspace(0.75, 1.5,750)];
ysi = akima(H,I,xi);

% remove the % sign in the line below to enable the plot function
% plot(H,I,'o',xi,ysi,':')

% get bcw

[ymin,i] = min(ysi);
bcw = xi(i);

% get depth

depth = 1 - ysi(i);

% get FWHM uses Petr Mikulik m file for FWHM calculation

z = ones(1,750);
```

```

aa = z.- ysi';
x = xi(1:750);
y = aa(1:750);

width = fwhm(x,y);

% build up data matrices

BCW(r,c) = bcw;
DEPTH(r,c) = depth;
FWHM(r,c) = width;

bcw;
depth;
width;

endfor

% *****

% save map images

save ("-text", "bandcenter", "BCW");
save ("-text", "banddepth", "DEPTH");
save ("-text", "fwhm", "FWHM");

```

Octave Program Code for Applycoeff.m:

```
% matrix regression Clementine Imagery for elemental abundance of Fe,  
Mg, Ca, Ti, Al, O
```

```
a = dlmread("banddepth.txt");
```

```
b = dlmread("bandcenter.txt");
```

```
c=dlmread("fwhm.txt");
```

```
d1=dlmread("1500.txt");
```

```
d2=dlmread("750.txt");
```

```
d = (d1 - d2)/1000;
```

```
aa=a.*a;
```

```
ab=a.*b;
```

```
ac=a.*c;
```

```
ad=a.*d;
```

```
bb=b.*b;
```

```
bc=b.*c;
```

```
bd=b.*d;
```

```
cc=c.*c;
```

```
cd=c.*d;
```

```
dd=d.*d;
```

```
% load matrix coefficients for Fe
```

```
load("matrix001","A");

% multiply coefficients

a=A(1,1).*a;
b=A(1,2).*b;
c=A(1,3).*c;
d=A(1,4).*d;

aa=A(1,5).*aa;
ab=A(1,6).*ab;
ac=A(1,7).*ac;
ad=A(1,8).*ad;

bb=A(1,9).*bb;
bc=A(1,10).*bc;
bd=A(1,11).*bd;

cc=A(1,12).*cc;
cd=A(1,13).*cd;

dd=A(1,14).*dd;

% sum M images and add offset coefficient

M=a+b+c+d+aa+ab+ac+ad+bb+bc+bd+cc+cd+dd;
```

```
Fe= M + A(1,15);

% save Fe matrix as matrix 002

filename = sprintf('matrix%03d.mat',2);

save(filename,'Fe')

% repeat for magnesium

a = dlmread("banddepth.txt");
b = dlmread("bandcenter.txt");
c=dlmread("fwhm.txt");
d1=dlmread("1500.txt");
d2=dlmread("750.txt");
d = (d1 - d2)/1000;

aa=a.*a;
ab=a.*b;
ac=a.*c;
ad=a.*d;

bb=b.*b;
bc=b.*c;
bd=b.*d;
cc=c.*c;
cd=c.*d;
```

```
dd=d.*d;

% load matrix coefficients for Mg

load("matrix003","A");

% multiply coefficients

a=A(1,1).*a;
b=A(1,2).*b;
c=A(1,3).*c;
d=A(1,4).*d;

aa=A(1,5).*aa;
ab=A(1,6).*ab;
ac=A(1,7).*ac;
ad=A(1,8).*ad;

bb=A(1,9).*bb;
bc=A(1,10).*bc;
bd=A(1,11).*bd;

cc=A(1,12).*cc;
cd=A(1,13).*cd;

dd=A(1,14).*dd;
```

```
% sum M images and add offset coefficient
```

```
M=a+b+c+d+aa+ab+ac+ad+bb+bc+bd+cc+cd+dd;
```

```
Mg= M + A(1,15);
```

```
% save Mg matrix as matrix 004
```

```
filename = sprintf('matrix%03d.mat',4);
```

```
save(filename,'Mg')
```

```
% repeat for calcium
```

```
a = dlmread("banddepth.txt");
```

```
b = dlmread("bandcenter.txt");
```

```
c=dlmread("fwhm.txt");
```

```
d1=dlmread("1500.txt");
```

```
d2=dlmread("750.txt");
```

```
d = (d1 - d2)/1000;
```

```
aa=a.*a;
```

```
ab=a.*b;
```

```
ac=a.*c;
```

```
ad=a.*d;
```

```
bb=b.*b;
bc=b.*c;
bd=b.*d;

cc=c.*c;
cd=c.*d;

dd=d.*d;

% load matrix coefficients for Ca

load("matrix005","A");

% multiply coefficients

a=A(1,1).*a;
b=A(1,2).*b;
c=A(1,3).*c;
d=A(1,4).*d;

aa=A(1,5).*aa;
ab=A(1,6).*ab;
ac=A(1,7).*ac;
ad=A(1,8).*ad;

bb=A(1,9).*bb;
```

```
bc=A(1,10).*bc;
bd=A(1,11).*bd;

cc=A(1,12).*cc;
cd=A(1,13).*cd;

dd=A(1,14).*dd;

% sum M images and add offset coefficient

M=a+b+c+d+aa+ab+ac+ad+bb+bc+bd+cc+cd+dd;
Ca= M + A(1,15);

% save Ca matrix as matrix 006

filename = sprintf('matrix%03d.mat',6);

save(filename,'Ca')

% repeat for Ti

a = dlmread("banddepth.txt");
b = dlmread("bandcenter.txt");
c=dlmread("fwhm.txt");
d1=dlmread("1500.txt");
d2=dlmread("750.txt");
d = (d1 - d2)/1000;
```

```
aa=a.*a;
ab=a.*b;
ac=a.*c;
ad=a.*d;

bb=b.*b;
bc=b.*c;
bd=b.*d;

cc=c.*c;
cd=c.*d;

dd=d.*d;

% load matrix coefficients for Ti

a = dlmread("banddepth.txt");
b = dlmread("bandcenter.txt");
c=dlmread("fwhm.txt");
d1=dlmread("1500.txt");
d2=dlmread("750.txt");
d = (d1 - d2)/1000;

aa=a.*a;
ab=a.*b;
ac=a.*c;
```

```
ad=a.*d;
```

```
bb=b.*b;
```

```
bc=b.*c;
```

```
bd=b.*d;
```

```
cc=c.*c;
```

```
cd=c.*d;
```

```
dd=d.*d;
```

```
load("matrix007","A");
```

```
% multiply coefficients
```

```
a=A(1,1).*a;
```

```
b=A(1,2).*b;
```

```
c=A(1,3).*c;
```

```
d=A(1,4).*d;
```

```
aa=A(1,5).*aa;
```

```
ab=A(1,6).*ab;
```

```
ac=A(1,7).*ac;
```

```
ad=A(1,8).*ad;
```

```
bb=A(1,9).*bb;
```

```
bc=A(1,10).*bc;
```

```
bd=A(1,11).*bd;

cc=A(1,12).*cc;
cd=A(1,13).*cd;

dd=A(1,14).*dd;

% sum M images and add offset coefficient

M=a+b+c+d+aa+ab+ac+ad+bb+bc+bd+cc+cd+dd;
Ti= M + A(1,15);

% save Ti matrix as matrix 008

filename = sprintf('matrix%03d.mat',8);

save(filename,'Ti')

% repeat for A1

a = dlmread("banddepth.txt");
b = dlmread("bandcenter.txt");
c=dlmread("fwhm.txt");
d1=dlmread("1500.txt");
d2=dlmread("750.txt");
d = (d1 - d2)/1000;
```

```
aa=a.*a;
```

```
ab=a.*b;
```

```
ac=a.*c;
```

```
ad=a.*d;
```

```
bb=b.*b;
```

```
bc=b.*c;
```

```
bd=b.*d;
```

```
cc=c.*c;
```

```
cd=c.*d;
```

```
dd=d.*d;
```

```
% load matrix coefficients for A1
```

```
a = dlmread("banddepth.txt");
```

```
b = dlmread("bandcenter.txt");
```

```
c=dlmread("fwhm.txt");
```

```
d1=dlmread("1500.txt");
```

```
d2=dlmread("750.txt");
```

```
d = (d1 - d2)/1000;
```

```
aa=a.*a;
```

```
ab=a.*b;
```

```
ac=a.*c;
```

```
ad=a.*d;

bb=b.*b;
bc=b.*c;
bd=b.*d;

cc=c.*c;
cd=c.*d;

dd=d.*d;

load("matrix009","A");

% multiply coefficients

a=A(1,1).*a;
b=A(1,2).*b;
c=A(1,3).*c;
d=A(1,4).*d;

aa=A(1,5).*aa;
ab=A(1,6).*ab;
ac=A(1,7).*ac;
ad=A(1,8).*ad;

bb=A(1,9).*bb;
bc=A(1,10).*bc;
```

```
bd=A(1,11).*bd;

cc=A(1,12).*cc;
cd=A(1,13).*cd;

dd=A(1,14).*dd;

% sum M images and add offset coefficient

M=a+b+c+d+aa+ab+ac+ad+bb+bc+bd+cc+cd+dd;
A1= M + A(1,15);

% save A1 matrix as matrix 010

filename = sprintf('matrix%03d.mat',10);

save(filename,'A1')

% repeat for 0

a = dlmread("banddepth.txt");
b = dlmread("bandcenter.txt");
c=dlmread("fwhm.txt");
d1=dlmread("1500.txt");
d2=dlmread("750.txt");
d = (d1 - d2)/1000;
```

```
aa=a.*a;
ab=a.*b;
ac=a.*c;
ad=a.*d;

bb=b.*b;
bc=b.*c;
bd=b.*d;

cc=c.*c;
cd=c.*d;

dd=d.*d;

% load matrix coefficients for 0
a = dlmread("banddepth.txt");
b = dlmread("bandcenter.txt");
c=dlmread("fwhm.txt");
d1=dlmread("1500.txt");
d2=dlmread("750.txt");
d = (d1 - d2)/1000;

aa=a.*a;
ab=a.*b;
ac=a.*c;
ad=a.*d;
```

```
bb=b.*b;
bc=b.*c;
bd=b.*d;

cc=c.*c;
cd=c.*d;

dd=d.*d;

load("matrix011","A");

% multiply coefficients

a=A(1,1).*a;
b=A(1,2).*b;
c=A(1,3).*c;
d=A(1,4).*d;

aa=A(1,5).*aa;
ab=A(1,6).*ab;
ac=A(1,7).*ac;
ad=A(1,8).*ad;

bb=A(1,9).*bb;
bc=A(1,10).*bc;
bd=A(1,11).*bd;
```

```
cc=A(1,12).*cc;
cd=A(1,13).*cd;

dd=A(1,14).*dd;

% sum M images and add offset coefficient

M=a+b+c+d+aa+ab+ac+ad+bb+bc+bd+cc+cd+dd;
O= M + A(1,15);

% save O matrix as matrix 012

filename = sprintf('matrix%03d.mat',12);

save(filename,'O')
```

Octave Code for newmatreg_v3.m

```
% matrix regression Clementine Imagery for elemental abundance of Iron
```

```
a = dlmread('banddepth.txt');
```

```
b = dlmread('bandcenter.txt');
```

```
c=dlmread('fwhm.txt');
```

```
d1=dlmread('1500.txt');
```

```
d2=dlmread('750.txt');
```

```
B=dlmread('LPFe.txt');
```

```
d=(d1 - d2)/1000;
```

```
% create row vectors
```

```
[nr,nc] = size(a);
```

```
length = nr* nc;
```

```
a = reshape(a,1,length);
```

```
b= reshape(b,1,length);
```

```
c=reshape(c,1,length);
```

```
d=reshape(d,1,length);
```

```
% exclude bad Clementine pixels
```

```
idx=find(a<0.2);
```

```
a=a(idx);
```

```
b=b(idx);
```

```
c=c(idx);
```

```

d=d(idx);

aa=a.*a;
ab=a.*b;
ac=a.*c;
ad=a.*d;
bb=b.*b;
bc=b.*c;
bd=b.*d;
cc=c.*c;
cd=c.*d;
dd=d.*d;

B=reshape(B,1,length);
e=ones(1,length);
B=B(idx);
e=e(idx);

% create x matrix
x = [a;b;c;d;aa;ab;ac;ad;bb;bc;bd;cc;cd;dd;e];

% create coefficient matrix
A = mrdivide(B,x);
rmse = sqrt(mean((A*x-B).^2));
fprintf('RMSE(Fe) = %f\n',rmse);
filename = sprintf('matrix%03d.mat',1);
save(filename,'A')

```

```
% repeat for magnesium

B=dlmread('LPMg.txt');
B=reshape(B,1,length);
e=ones(1,length);
B=B(idx);
e=e(idx);

% create coefficient matrix
A = mrdivide(B,x);
rmse = sqrt(mean((A*x-B).^2));
fprintf('RMSE(Mg) = %f\n',rmse);
filename = sprintf('matrix%03d.mat',3);
save(filename,'A')

% repeat for calcium

B=dlmread('LPCa.txt');
B=reshape(B,1,length);
e=ones(1,length);
B=B(idx);
e=e(idx);

% create coefficient matrix
A = mrdivide(B,x);
rmse = sqrt(mean((A*x-B).^2));
```

```

fprintf('RMSE(Ca) = %f\n',rmse);

filename = sprintf('matrix%03d.mat',5);

save(filename,'A')

% repeat for Ti

B=dlmread('LPTi.txt');

B=reshape(B,1,length);

e=ones(1,length);

B=B(idx);

e=e(idx);

% create coefficient matrix

A = mrdivide(B,x);

rmse = sqrt(mean((A*x-B).^2));

fprintf('RMSE(Ti) = %f\n',rmse);

filename = sprintf('matrix%03d.mat',7);

save(filename,'A')

% repeat for Al

B=dlmread('LPA1.txt');

B=reshape(B,1,length);

e=ones(1,length);

B=B(idx);

```

```

e=e(idx);

% create coefficient matrix
A = mrdivide(B,x);
rmse = sqrt(mean((A*x-B).^2));
fprintf('RMSE(A1) = %f\n',rmse);
filename = sprintf('matrix%03d.mat',9);
save(filename,'A')

% repeat for 0

B=dlmread('LPO.txt');
B=reshape(B,1,length);
e=ones(1,length);
B=B(idx);
e=e(idx);

% create coefficient matrix
A = mrdivide(B,x);
rmse = sqrt(mean((A*x-B).^2));
fprintf('RMSE(O) = %f\n',rmse);
filename = sprintf('matrix%03d.mat',11);
save(filename,'A')

```

Petrologic Mapping: applycoeff_v2.m and read_from_ternary_diagram.m

This specialty version of applycoeff.m uses three endmember data to produce a petrographic map. The resulting petrographic map is saved as a 24-bit colour TIFF file named "petrographic_map.tif", in which the red, green, and blue channel represents the mare basalt, Mg-rich rock, and FAN endmember, respectively. The sum of the channels is always 255, as the endmember abundances always must sum up to 1. For Reiner Gamma, we have mostly mare basalt, some Mg-rich rock, and nearly no FAN; that's why the petrographic map looks red-orange. Both m files must be in the same directory as the input image files and matrix files.

applycoeff_v2.m

```
% matrix regression Clementine Imagery for elemental abundance of Fe,  
Mg, Ca, Ti, Al, O
```

```
a = dlmread("banddepth.txt");  
b = dlmread("bandcenter.txt");  
c=dlmread("fwhm.txt");  
d1=dlmread("1500.txt");  
d2=dlmread("750.txt");  
d = (d1 - d2)/1000;  
  
aa=a.*a;  
ab=a.*b;  
ac=a.*c;  
ad=a.*d;
```

```
bb=b.*b;
```

```
bc=b.*c;
```

```
bd=b.*d;
```

```
cc=c.*c;
```

```
cd=c.*d;
```

```
dd=d.*d;
```

```
% load matrix coefficients for Fe
```

```
load("matrix001","A");
```

```
% multiply coefficients
```

```
a=A(1,1).*a;
```

```
b=A(1,2).*b;
```

```
c=A(1,3).*c;
```

```
d=A(1,4).*d;
```

```
aa=A(1,5).*aa;
```

```
ab=A(1,6).*ab;
```

```
ac=A(1,7).*ac;
```

```
ad=A(1,8).*ad;
```

```
bb=A(1,9).*bb;
```

```
bc=A(1,10).*bc;
bd=A(1,11).*bd;

cc=A(1,12).*cc;
cd=A(1,13).*cd;

dd=A(1,14).*dd;

% sum M images and add offset coefficient

M=a+b+c+d+aa+ab+ac+ad+bb+bc+bd+cc+cd+dd;
Fe= M + A(1,15);

% save Fe matrix as matrix 002

filename = sprintf('matrix%03d.mat',2);

save(filename,'Fe')

% repeat for magnesium

a = dlmread("banddepth.txt");
b = dlmread("bandcenter.txt");
c=dlmread("fwhm.txt");
d1=dlmread("1500.txt");
d2=dlmread("750.txt");
```

```
d = (d1 - d2)/1000;
```

```
aa=a.*a;
```

```
ab=a.*b;
```

```
ac=a.*c;
```

```
ad=a.*d;
```

```
bb=b.*b;
```

```
bc=b.*c;
```

```
bd=b.*d;
```

```
cc=c.*c;
```

```
cd=c.*d;
```

```
dd=d.*d;
```

```
% load matrix coefficients for Mg
```

```
load("matrix003","A");
```

```
% multiply coefficients
```

```
a=A(1,1).*a;
```

```
b=A(1,2).*b;
```

```
c=A(1,3).*c;
```

```
d=A(1,4).*d;
```

```
aa=A(1,5).*aa;
ab=A(1,6).*ab;
ac=A(1,7).*ac;
ad=A(1,8).*ad;

bb=A(1,9).*bb;
bc=A(1,10).*bc;
bd=A(1,11).*bd;

cc=A(1,12).*cc;
cd=A(1,13).*cd;

dd=A(1,14).*dd;

% sum M images and add offset coefficient

M=a+b+c+d+aa+ab+ac+ad+bb+bc+bd+cc+cd+dd;

Mg= M + A(1,15);

% save Mg matrix as matrix 004

filename = sprintf('matrix%03d.mat',4);

save(filename,'Mg')

% repeat for calcium
```

```
a = dlmread("banddepth.txt");
b = dlmread("bandcenter.txt");
c=dlmread("fwhm.txt");
d1=dlmread("1500.txt");
d2=dlmread("750.txt");
d = (d1 - d2)/1000;

aa=a.*a;
ab=a.*b;
ac=a.*c;
ad=a.*d;

bb=b.*b;
bc=b.*c;
bd=b.*d;

cc=c.*c;
cd=c.*d;

dd=d.*d;

% load matrix coefficients for Ca

load("matrix005","A");
```

```
% multiply coefficients

a=A(1,1).*a;
b=A(1,2).*b;
c=A(1,3).*c;
d=A(1,4).*d;

aa=A(1,5).*aa;
ab=A(1,6).*ab;
ac=A(1,7).*ac;
ad=A(1,8).*ad;

bb=A(1,9).*bb;
bc=A(1,10).*bc;
bd=A(1,11).*bd;

cc=A(1,12).*cc;
cd=A(1,13).*cd;

dd=A(1,14).*dd;

% sum M images and add offset coefficient

M=a+b+c+d+aa+ab+ac+ad+bb+bc+bd+cc+cd+dd;

Ca= M + A(1,15);

% save Ca matrix as matrix 006
```

```
filename = sprintf('matrix%03d.mat',6);
```

```
save(filename,'Ca')
```

```
% repeat for Ti
```

```
a = dlmread("banddepth.txt");
```

```
b = dlmread("bandcenter.txt");
```

```
c=dlmread("fwhm.txt");
```

```
d1=dlmread("1500.txt");
```

```
d2=dlmread("750.txt");
```

```
d = (d1 - d2)/1000;
```

```
aa=a.*a;
```

```
ab=a.*b;
```

```
ac=a.*c;
```

```
ad=a.*d;
```

```
bb=b.*b;
```

```
bc=b.*c;
```

```
bd=b.*d;
```

```
cc=c.*c;
```

```
cd=c.*d;
```

```
dd=d.*d;
```

```
% load matrix coefficients for Ti

a = dlmread("banddepth.txt");
b = dlmread("bandcenter.txt");
c=dlmread("fwhm.txt");
d1=dlmread("1500.txt");
d2=dlmread("750.txt");
d = (d1 - d2)/1000;

aa=a.*a;
ab=a.*b;
ac=a.*c;
ad=a.*d;

bb=b.*b;
bc=b.*c;
bd=b.*d;

cc=c.*c;
cd=c.*d;

dd=d.*d;

load("matrix007","A");

% multiply coefficients
```

```
a=A(1,1).*a;
b=A(1,2).*b;
c=A(1,3).*c;
d=A(1,4).*d;

aa=A(1,5).*aa;
ab=A(1,6).*ab;
ac=A(1,7).*ac;
ad=A(1,8).*ad;

bb=A(1,9).*bb;
bc=A(1,10).*bc;
bd=A(1,11).*bd;

cc=A(1,12).*cc;
cd=A(1,13).*cd;

dd=A(1,14).*dd;

% sum M images and add offset coefficient

M=a+b+c+d+aa+ab+ac+ad+bb+bc+bd+cc+cd+dd;

Ti= M + A(1,15);

% save Ti matrix as matrix 008
```

```
filename = sprintf('matrix%03d.mat',8);

save(filename,'Ti')

% repeat for Al

a = dlmread("banddepth.txt");
b = dlmread("bandcenter.txt");
c=dlmread("fwhm.txt");
d1=dlmread("1500.txt");
d2=dlmread("750.txt");
d = (d1 - d2)/1000;

aa=a.*a;
ab=a.*b;
ac=a.*c;
ad=a.*d;

bb=b.*b;
bc=b.*c;
bd=b.*d;

cc=c.*c;
cd=c.*d;

dd=d.*d;
```

```
% load matrix coefficients for A1
```

```
a = dlmread("banddepth.txt");
```

```
b = dlmread("bandcenter.txt");
```

```
c=dlmread("fwhm.txt");
```

```
d1=dlmread("1500.txt");
```

```
d2=dlmread("750.txt");
```

```
d = (d1 - d2)/1000;
```

```
aa=a.*a;
```

```
ab=a.*b;
```

```
ac=a.*c;
```

```
ad=a.*d;
```

```
bb=b.*b;
```

```
bc=b.*c;
```

```
bd=b.*d;
```

```
cc=c.*c;
```

```
cd=c.*d;
```

```
dd=d.*d;
```

```
load("matrix009","A");
```

```
% multiply coefficients
```

```
a=A(1,1).*a;
b=A(1,2).*b;
c=A(1,3).*c;
d=A(1,4).*d;

aa=A(1,5).*aa;
ab=A(1,6).*ab;
ac=A(1,7).*ac;
ad=A(1,8).*ad;

bb=A(1,9).*bb;
bc=A(1,10).*bc;
bd=A(1,11).*bd;

cc=A(1,12).*cc;
cd=A(1,13).*cd;

dd=A(1,14).*dd;

% sum M images and add offset coefficient

M=a+b+c+d+aa+ab+ac+ad+bb+bc+bd+cc+cd+dd;

A1= M + A(1,15);

% save A1 matrix as matrix 010

filename = sprintf('matrix%03d.mat',10);
```

```
save(filename, 'A1')

% repeat for 0

a = dlmread("banddepth.txt");
b = dlmread("bandcenter.txt");
c=dlmread("fwhm.txt");
d1=dlmread("1500.txt");
d2=dlmread("750.txt");
d = (d1 - d2)/1000;

aa=a.*a;
ab=a.*b;
ac=a.*c;
ad=a.*d;

bb=b.*b;
bc=b.*c;
bd=b.*d;

cc=c.*c;
cd=c.*d;

dd=d.*d;
```

```
% load matrix coefficients for O
a = dlmread("banddepth.txt");
b = dlmread("bandcenter.txt");
c=dlmread("fwhm.txt");
d1=dlmread("1500.txt");
d2=dlmread("750.txt");
d = (d1 - d2)/1000;

aa=a.*a;
ab=a.*b;
ac=a.*c;
ad=a.*d;

bb=b.*b;
bc=b.*c;
bd=b.*d;

cc=c.*c;
cd=c.*d;

dd=d.*d;

load("matrix011","A");

% multiply coefficients
a=A(1,1).*a;
b=A(1,2).*b;
```

```
c=A(1,3).*c;
d=A(1,4).*d;

aa=A(1,5).*aa;
ab=A(1,6).*ab;
ac=A(1,7).*ac;
ad=A(1,8).*ad;

bb=A(1,9).*bb;
bc=A(1,10).*bc;
bd=A(1,11).*bd;

cc=A(1,12).*cc;
cd=A(1,13).*cd;

dd=A(1,14).*dd;

% sum M images and add offset coefficient

M=a+b+c+d+aa+ab+ac+ad+bb+bc+bd+cc+cd+dd;
O= M + A(1,15);

% save Fe matrix as matrix 012

filename = sprintf('matrix%03d.mat',12);
```

```
save(filename,'O');

% compute petrographic map

fan_fe=0.0050;

fan_mg=0.0100;

mb_fe=0.1800;

mb_mg=0.0650;

mgs_fe=0.0400;

mgs_mg=0.1300;

f=read_from_ternary_diagram([fan_fe; fan_mg],[mb_fe; mb_mg],[mgs_fe;
mgs_mg],0.01.*Fe(:),0.01.*Mg(:));

[nr,nc]=size(Fe);

bas=reshape(f(2,:),nr,nc); % mare basalt

mgr=reshape(f(3,:),nr,nc); % Mg-rich rock

fan=reshape(f(1,:),nr,nc); % FAN

pm=zeros(nr,nc,3);

pm(:,:,1)=bas;

pm(:,:,2)=mgr;

pm(:,:,3)=fan;

imwrite(pm,'petrographic_map.tif');
```

**Program code for applycoeff_v3a.m which maps variations
in mare basalt composition:**

```
% matrix regression Clementine Imagery for elemental abundance of Fe,  
Mg, Ca, Ti, Al, O
```

```
a = dlmread("banddepth.txt");
```

```
b = dlmread("bandcenter.txt");
```

```
c=dlmread("fwhm.txt");
```

```
d1=dlmread("1500.txt");
```

```
d2=dlmread("750.txt");
```

```
d = (d1 - d2)/1000;
```

```
aa=a.*a;
```

```
ab=a.*b;
```

```
ac=a.*c;
```

```
ad=a.*d;
```

```
bb=b.*b;
```

```
bc=b.*c;
```

```
bd=b.*d;
```

```
cc=c.*c;
```

```
cd=c.*d;
```

```
dd=d.*d;
```

```
% load matrix coefficients for Fe
```

```
load("matrix001","A");
```

```
% multiply coefficients
```

```
a=A(1,1).*a;
```

```
b=A(1,2).*b;
```

```
c=A(1,3).*c;
```

```
d=A(1,4).*d;
```

```
aa=A(1,5).*aa;
```

```
ab=A(1,6).*ab;
```

```
ac=A(1,7).*ac;
```

```
ad=A(1,8).*ad;
```

```
bb=A(1,9).*bb;
```

```
bc=A(1,10).*bc;
```

```
bd=A(1,11).*bd;
```

```
cc=A(1,12).*cc;
```

```
cd=A(1,13).*cd;
```

```
dd=A(1,14).*dd;
```

```
% sum M images and add offset coefficient
```

```
M=a+b+c+d+aa+ab+ac+ad+bb+bc+bd+cc+cd+dd;
```

```
Fe= M + A(1,15);
```

```
% save Fe matrix as matrix 002
```

```
filename = sprintf('matrix%03d.mat',2);
```

```
save(filename,'Fe')
```

```
% repeat for magnesium
```

```
a = dlmread("banddepth.txt");
```

```
b = dlmread("bandcenter.txt");
```

```
c=dlmread("fwhm.txt");
```

```
d1=dlmread("1500.txt");
```

```
d2=dlmread("750.txt");
```

```
d = (d1 - d2)/1000;
```

```
aa=a.*a;
```

```
ab=a.*b;
```

```
ac=a.*c;
```

```
ad=a.*d;
```

```
bb=b.*b;
```

```
bc=b.*c;
bd=b.*d;

cc=c.*c;
cd=c.*d;

dd=d.*d;

% load matrix coefficients for Mg

load("matrix003","A");

% multiply coefficients

a=A(1,1).*a;
b=A(1,2).*b;
c=A(1,3).*c;
d=A(1,4).*d;

aa=A(1,5).*aa;
ab=A(1,6).*ab;
ac=A(1,7).*ac;
ad=A(1,8).*ad;

bb=A(1,9).*bb;
bc=A(1,10).*bc;
bd=A(1,11).*bd;
```

```
cc=A(1,12).*cc;
cd=A(1,13).*cd;

dd=A(1,14).*dd;

% sum M images and add offset coefficient

M=a+b+c+d+aa+ab+ac+ad+bb+bc+bd+cc+cd+dd;
Mg= M + A(1,15);

% save Mg matrix as matrix 004

filename = sprintf('matrix%03d.mat',4);

save(filename,'Mg')

% repeat for calcium

a = dlmread("banddepth.txt");
b = dlmread("bandcenter.txt");
c=dlmread("fwhm.txt");
d1=dlmread("1500.txt");
d2=dlmread("750.txt");
d = (d1 - d2)/1000;
```

```
aa=a.*a;
ab=a.*b;
ac=a.*c;
ad=a.*d;

bb=b.*b;
bc=b.*c;
bd=b.*d;

cc=c.*c;
cd=c.*d;

dd=d.*d;

% load matrix coefficients for Ca

load("matrix005","A");

% multiply coefficients

a=A(1,1).*a;
b=A(1,2).*b;
c=A(1,3).*c;
d=A(1,4).*d;
```

```
aa=A(1,5).*aa;
ab=A(1,6).*ab;
ac=A(1,7).*ac;
ad=A(1,8).*ad;

bb=A(1,9).*bb;
bc=A(1,10).*bc;
bd=A(1,11).*bd;

cc=A(1,12).*cc;
cd=A(1,13).*cd;

dd=A(1,14).*dd;

% sum M images and add offset coefficient

M=a+b+c+d+aa+ab+ac+ad+bb+bc+bd+cc+cd+dd;

Ca= M + A(1,15);

% save Ca matrix as matrix 006

filename = sprintf('matrix%03d.mat',6);

save(filename,'Ca')

% repeat for Ti
```

```
a = dlmread("banddepth.txt");
b = dlmread("bandcenter.txt");
c=dlmread("fwhm.txt");
d1=dlmread("1500.txt");
d2=dlmread("750.txt");
d = (d1 - d2)/1000;

aa=a.*a;
ab=a.*b;
ac=a.*c;
ad=a.*d;

bb=b.*b;
bc=b.*c;
bd=b.*d;

cc=c.*c;
cd=c.*d;

dd=d.*d;

% load matrix coefficients for Ti

a = dlmread("banddepth.txt");
b = dlmread("bandcenter.txt");
c=dlmread("fwhm.txt");
d1=dlmread("1500.txt");
```

```
d2=dlmread("750.txt");
```

```
d = (d1 - d2)/1000;
```

```
aa=a.*a;
```

```
ab=a.*b;
```

```
ac=a.*c;
```

```
ad=a.*d;
```

```
bb=b.*b;
```

```
bc=b.*c;
```

```
bd=b.*d;
```

```
cc=c.*c;
```

```
cd=c.*d;
```

```
dd=d.*d;
```

```
load("matrix007","A");
```

```
% multiply coefficients
```

```
a=A(1,1).*a;
```

```
b=A(1,2).*b;
```

```
c=A(1,3).*c;
```

```
d=A(1,4).*d;
```

```
aa=A(1,5).*aa;
```

```
ab=A(1,6).*ab;
ac=A(1,7).*ac;
ad=A(1,8).*ad;

bb=A(1,9).*bb;
bc=A(1,10).*bc;
bd=A(1,11).*bd;

cc=A(1,12).*cc;
cd=A(1,13).*cd;

dd=A(1,14).*dd;

% sum M images and add offset coefficient

M=a+b+c+d+aa+ab+ac+ad+bb+bc+bd+cc+cd+dd;

Ti= M + A(1,15);

% save Ti matrix as matrix 008

filename = sprintf('matrix%03d.mat',8);

save(filename,'Ti')

% repeat for A1
```

```
a = dlmread("banddepth.txt");
b = dlmread("bandcenter.txt");
c=dlmread("fwhm.txt");
d1=dlmread("1500.txt");
d2=dlmread("750.txt");
d = (d1 - d2)/1000;
```

```
aa=a.*a;
ab=a.*b;
ac=a.*c;
ad=a.*d;
```

```
bb=b.*b;
bc=b.*c;
bd=b.*d;
```

```
cc=c.*c;
cd=c.*d;
```

```
dd=d.*d;
```

```
% load matrix coefficients for A1
```

```
a = dlmread("banddepth.txt");
b = dlmread("bandcenter.txt");
c=dlmread("fwhm.txt");
d1=dlmread("1500.txt");
d2=dlmread("750.txt");
```

```
d = (d1 - d2)/1000;

aa=a.*a;
ab=a.*b;
ac=a.*c;
ad=a.*d;

bb=b.*b;
bc=b.*c;
bd=b.*d;

cc=c.*c;
cd=c.*d;

dd=d.*d;

load("matrix009","A");

% multiply coefficients

a=A(1,1).*a;
b=A(1,2).*b;
c=A(1,3).*c;
d=A(1,4).*d;

aa=A(1,5).*aa;
ab=A(1,6).*ab;
```

```
ac=A(1,7).*ac;
ad=A(1,8).*ad;

bb=A(1,9).*bb;
bc=A(1,10).*bc;
bd=A(1,11).*bd;

cc=A(1,12).*cc;
cd=A(1,13).*cd;

dd=A(1,14).*dd;

% sum M images and add offset coefficient

M=a+b+c+d+aa+ab+ac+ad+bb+bc+bd+cc+cd+dd;

A1= M + A(1,15);

% save A1 matrix as matrix 010

filename = sprintf('matrix%03d.mat',10);

save(filename,'A1')

% repeat for 0

a = dlmread("banddepth.txt");
b = dlmread("bandcenter.txt");
```

```
c=dlmread("fwhm.txt");
d1=dlmread("1500.txt");
d2=dlmread("750.txt");
d = (d1 - d2)/1000;

aa=a.*a;
ab=a.*b;
ac=a.*c;
ad=a.*d;

bb=b.*b;
bc=b.*c;
bd=b.*d;

cc=c.*c;
cd=c.*d;

dd=d.*d;

% load matrix coefficients for O
a = dlmread("banddepth.txt");
b = dlmread("bandcenter.txt");
c=dlmread("fwhm.txt");
d1=dlmread("1500.txt");
d2=dlmread("750.txt");
d = (d1 - d2)/1000;
```

```
aa=a.*a;
ab=a.*b;
ac=a.*c;
ad=a.*d;

bb=b.*b;
bc=b.*c;
bd=b.*d;

cc=c.*c;
cd=c.*d;

dd=d.*d;

load("matrix011","A");

% multiply coefficients

a=A(1,1).*a;
b=A(1,2).*b;
c=A(1,3).*c;
d=A(1,4).*d;

aa=A(1,5).*aa;
ab=A(1,6).*ab;
ac=A(1,7).*ac;
ad=A(1,8).*ad;
```

```
bb=A(1,9).*bb;
bc=A(1,10).*bc;
bd=A(1,11).*bd;

cc=A(1,12).*cc;
cd=A(1,13).*cd;

dd=A(1,14).*dd;

% sum M images and add offset coefficient

M=a+b+c+d+aa+ab+ac+ad+bb+bc+bd+cc+cd+dd;
O= M + A(1,15);

% save Fe matrix as matrix 012

filename = sprintf('matrix%03d.mat',12);

save(filename,'O');

% compute petrographic map
hiti_ti=0.036;
hiti_al=0.063;
mb_ti=0.016;
mb_al=0.0925;
```

```
aluminous_ti=0.00500;
aluminous_al=0.140;
f=read_from_ternary_diagram([hiti_ti; hiti_al],[mb_ti; mb_al],
[aluminous_ti; aluminous_al],0.01.*Ti(:),0.01.*Al(:));
[nr,nc]=size(Fe);
bas=reshape(f(2,:),nr,nc); % mare basalt
aluminous=reshape(f(3,:),nr,nc); % aluminous basalt
hiti=reshape(f(1,:),nr,nc); % hi titanium basalt
pm=zeros(nr,nc,3);
pm(:,:,1)=bas;
pm(:,:,2)=aluminous;
pm(:,:,3)=hiti;
imwrite(pm,'petrographic_map_basalt_3a.tif');
```

read_from_ternary_diagram.m

```
function f=read_from_ternary_diagram(e1,e2,e3,x,y)

% e1, e2, e3: three endmembers (2x1 vectors)

a12=(e2(2)-e1(2))/(e2(1)-e1(1));

b12=e2(2)-a12*e2(1);

n12=zeros(2,1);

n12(1)=a12/sqrt(1.0+a12*a12);

n12(2)=-1.0/sqrt(1.0+a12*a12);

p12=-b12/sqrt(1.0+a12*a12);

d3=e3(1)*n12(1)+e3(2)*n12(2)-p12;

a23=(e3(2)-e2(2))/(e3(1)-e2(1));

b23=e3(2)-a23*e3(1);

n23=zeros(2,1);

n23(1)=a23/sqrt(1.0+a23*a23);

n23(2)=-1.0/sqrt(1.0+a23*a23);

p23=-b23/sqrt(1.0+a23*a23);

d1=e1(1)*n23(1)+e1(2)*n23(2)-p23;

a13=(e3(2)-e1(2))/(e3(1)-e1(1));

b13=e3(2)-a13*e3(1);

n13=zeros(2,1);

n13(1)=a13/sqrt(1.0+a13*a13);

n13(2)=-1.0/sqrt(1.0+a13*a13);
```

```

p13=-b13/sqrt(1.0+a13*a13);
d2=e2(1)*n13(1)+e2(2)*n13(2)-p13;

% x, y: data points (nx1 vector)
n=length(x);
f=zeros(3,n);
for i=1:n
    h3=x(i)*n12(1)+y(i)*n12(2)-p12;
    f(3,i)=h3/d3;

    h1=x(i)*n23(1)+y(i)*n23(2)-p23;
    f(1,i)=h1/d1;

    h2=x(i)*n13(1)+y(i)*n13(2)-p13;
    f(2,i)=h2/d2;
end

% clipping to the interval [0,1]
for i=1:n
    for j=1:3
        if(f(j,i)<0.0)
            f(j,i)=0.0;
        end
        if(f(j,i)>1.0)
            f(j,i)=1.0;
        end
    end
end

```

```
end
```

```
% normalisation to 1
```

```
for i=1:n
```

```
    f(:,i)=f(:,i)/sum(f(:,i));
```

```
end
```

Octave code for Akima.m is available here:

<http://www.mathworks.in/matlabcentral/fileexchange/1814>

Octave code for fwhm.m is available here:

<http://octave.svn.sourceforge.net/viewvc/octave/trunk/octave-forge/main/signal/inst/?pathrev=6041>

Lunar Prospector global elemental abundance maps may be downloaded in asc format from here:

<http://www.mapaplanet.org/explorer/moon.html>